# Microfluidic viscometers for shear rheology of complex fluids and biofluids

Siddhartha Gupta, William S. Wang, and Siva A. Vanapalli

Citation: Biomicrofluidics **10**, 043402 (2016); doi: 10.1063/1.4955123
View online: http://dx.doi.org/10.1063/1.4955123
View Table of Contents: http://scitation.aip.org/content/aip/journal/bmf/10/4?ver=pdfcov
Published by the AIP Publishing

BIOMICROFLUIDICS **10**, 043402 (2016)

# Microfluidic viscometers for shear rheology of complex fluids and biofluids

Siddhartha Gupta, William S. Wang, and Siva A. Vanapalli[a)]
*Department of Chemical Engineering, Texas Tech University, Lubbock, Texas 79409, USA*

(Received 2 April 2016; accepted 21 June 2016; published online 5 July 2016)

The rich diversity of man-made complex fluids and naturally occurring biofluids is opening up new opportunities for investigating their flow behavior and characterizing their rheological properties. Steady shear viscosity is undoubtedly the most widely characterized material property of these fluids. Although widely adopted, macroscale rheometers are limited by sample volumes, access to high shear rates, hydrodynamic instabilities, and interfacial artifacts. Currently, microfluidic devices are capable of handling low sample volumes, providing precision control of flow and channel geometry, enabling a high degree of multiplexing and automation, and integrating flow visualization and optical techniques. These intrinsic advantages of microfluidics have made it especially suitable for the steady shear rheology of complex fluids. In this paper, we review the use of microfluidics for conducting shear viscometry of complex fluids and biofluids with a focus on viscosity curves as a function of shear rate. We discuss the physical principles underlying different microfluidic viscometers, their unique features and limits of operation. This compilation of technological options will potentially serve in promoting the benefits of microfluidic viscometry along with evincing further interest and research in this area. We intend that this review will aid researchers handling and studying complex fluids in selecting and adopting microfluidic viscometers based on their needs. We conclude with challenges and future directions in microfluidic rheometry of complex fluids and biofluids. *Published by AIP Publishing.* [http://dx.doi.org/10.1063/1.4955123]

## I. INTRODUCTION

Complex fluids are ubiquitous in our everyday life. Typical examples include engine oils, shaving cream, paints, and ketchup (see Fig. 1). A common feature of these complex fluids is that they all have a characteristic microstructure at length scales larger than the molecular scale but smaller than the macroscopic scale.[1] This mesoscale structure is a hallmark of complex fluids. For example, the mesoscale structure in milk is fat globules, which can be manipulated (by changing volume fraction and aggregation state of fat globules) to yield either cream or butter.[2] Alternatively, building blocks such as polymer molecules, surfactants, colloidal particles, and bubbles can be assembled to engineer a rich variety of complex fluids with unique microstructures.

An astonishing diversity of complex fluids also exists in biological systems that support specific functions in organisms.[3] Some of these are bodily fluids such as saliva, blood, vitreous humor, and synovial fluid (see Figs. 1(e)–1(h)), while others are more of "living" complex fluids such as microbial biofilms.[4] In this review, we collectively refer to these fluids of biological origin as biofluids. We do this merely to distinguish synthetic complex fluids from natural ones, since there is a great degree of overlap between the physical principles and methods employed to study both of these classes of fluids.

[a)]Author to whom correspondence should be addressed. Electronic mail: siva.vanapalli@ttu.edu

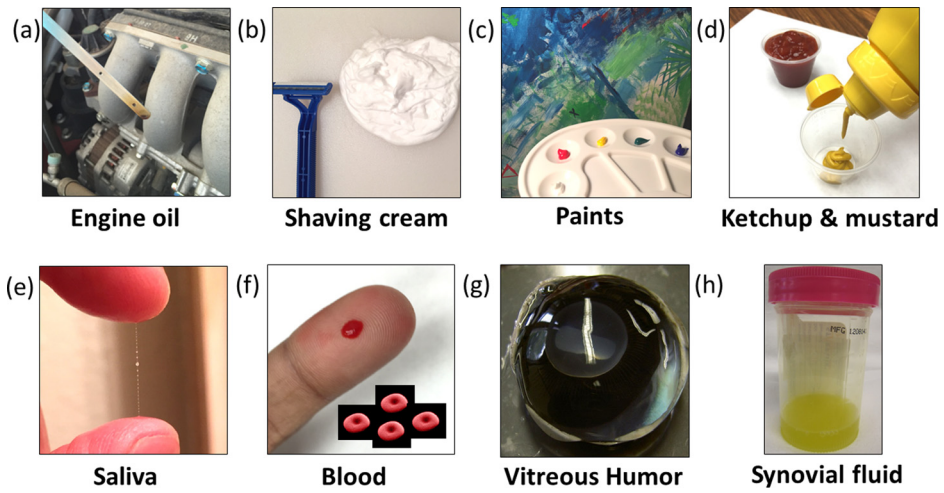


FIG. 1. Diverse examples of complex fluids and biofluids from everyday life. (a) Engine oil is a blend of heavy hydrocarbons, aromatics, and additives. (b) Shaving cream is a foam containing as much as 90% of air. (c) Paints are colloidal suspensions often admixed with polymers. (d) Ketchup and mustard sauce are complex mixtures of particulate matter and biopolymers. (e) Saliva showing beads-on-a-string phenomenon due to the presence of viscoelastic mucin polymers. (f) Blood is a suspension of cells with volume fractions close to 45%. The inset shows red blood cells that are typically 8 $\mu$m in diameter. (g) Vitreous humor in the anterior of a dissected calf eye with the lens and iris visible underneath it. Vitreous humor has 98%–99% of its volume as water and also contains cells, salts, sugars, and collagen. Photograph by Mark Fickett distributed under a CC-BY-SA 2.5 licence. (h) Synovial fluid is a non-Newtonian fluid found in the cavities of synovial joints. It is made of hyaluronic acid, lubricin, proteinases, and collagenases. Photograph by James Heilman distributed under a CC-BY-SA 3.0 licence.

The most striking feature of complex fluids and biofluids is their rheology or flow properties.[1,5] These fluids have properties in between liquids and solids, and their rheological behavior can range from viscoelastic fluids to soft solids. As a result, it has become common to refer to these rheologically diverse fluids collectively as soft matter. The response of these soft materials depends on the type of imposed deformation (e.g., steady vs. transient shear). Therefore, several material functions (e.g., shear/elongational viscosity, first/second normal stress coefficients, and storage/loss modulus)[6] are needed to thoroughly describe the rheological properties of complex fluids and biofluids.

Shear viscosity is undoubtedly the most widely characterized rheological property of complex fluids and biofluids. As shown in Fig. 2(a), the shear rheology of these fluids is central to numerous applications. The rheology of complex fluids is intimately dependent on shear rates. Depending on the processing condition, the shear rate can vary widely (see Fig. 2(a)), therefore, there is a need to characterize the shear rheology of complex fluids over a broad range. Likewise in biofluids, the shear viscosities vary widely as shown in Fig. 2(b). Often, the range of viscosities exhibited by biofluids is associated with a specific biological purpose. For example, the shear viscosity of blood decreases with increasing shear rate,[7] which is necessary for blood to flow through the smallest of capillaries and to deliver oxygen to surrounding cells and tissues. Thus, knowledge of shear rheology is important not only for optimizing processing/product performance in synthetic complex fluids but also for understanding physiological mechanisms and biological functions.

The sheer diversity of complex fluids and biofluids has continually led to the development of new methods to probe their rheology. In particular, recent advances in microfabrication and microfluidics have spurred the development of new tools to probe the rheology of complex fluids. Fundamental benefits of microfluidics include precision control of flow geometry and access to unique flow regimes and small length scales, while technological benefits include small sample volumes and parallel analysis. These broad benefits are driving widespread adoption of microfluidics to investigate the rheology of complex fluids and biofluids.

In this study, we review microfluidic shear viscometers for characterizing the shear rheology of complex fluids and biofluids. Early developments in the field have been reviewed by

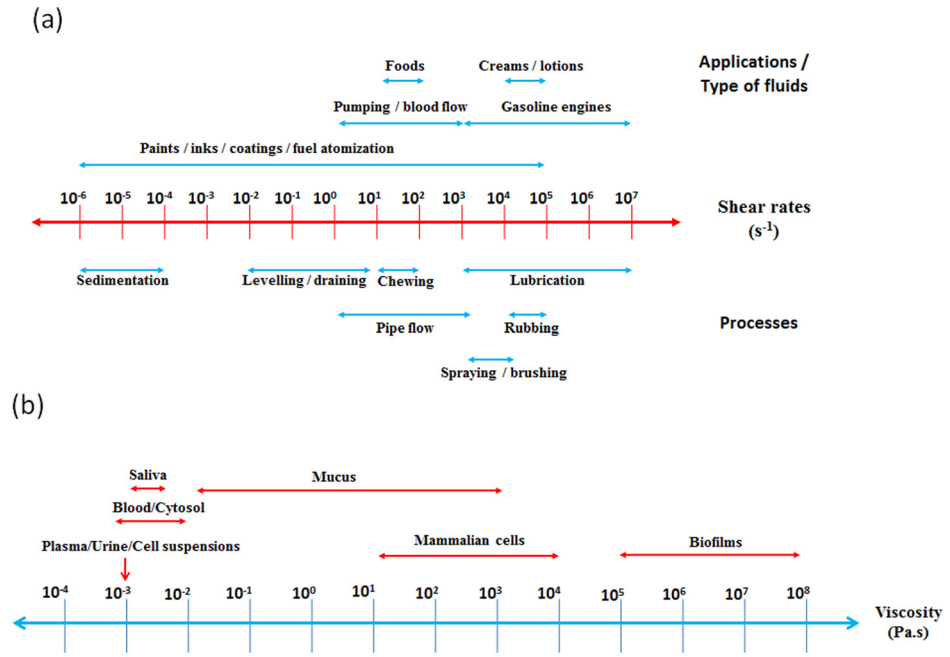


FIG. 2. Significance of shear rheology for complex fluids and biofluids. (a) Shear rate ranges for different applications alongside different processes in complex fluids. The range of shear rates varies widely from $10^{-6}$ to $10^{7}$ $s^{-1}$. From Barnes *et al.*, *An Introduction to Rheology*, Copyright 1989 John Wiley and Sons, Inc. Reprinted with permission from John Wiley and Sons, Inc. (b) Typical biofluids and their viscosity values,[19,121,134–140] showing the diversity in naturally occurring complex fluids.

Pipe and McKinley.[8] Microfluidic devices for extensional rheometry have also been reviewed recently.[9,10] The goal of this review is to present the latest advances in methods and devices that have been developed to measure the shear rheology of complex fluids and biofluids. We begin with fundamentals of shear viscometry (Sec. II), followed by limitations of macroscale shear rheometry (Sec. III). Subsequently, we elaborate on the significance and advantages of microfluidics for rheology (Sec. IV). In Sec. V, we discuss the basic principles of different microfluidic viscometry approaches, highlighting their methodology and key results. In Sec. VI, we discuss challenges and future directions for microfluidic shear viscometry and rheology, in general, and finally provide concluding remarks in Sec. VII.

## II. FUNDAMENTALS OF SHEAR VISCOMETRY

In this section, we discuss briefly the fundamentals of steady shear viscometry to introduce the reader to the concepts of viscosity and discuss how flow curves relating viscosity as a function of shear rate can be quantified from various viscometric flows. For a more detailed description of these concepts as well as how to characterize other material functions for complex fluids under various imposed flow kinematics, the reader is advised to refer to works by Macosko,[11] Morrison,[5,12] Barnes *et al.*,[13] and Larson.[1]

At the continuum scale, a fluid is assumed to be "smooth" everywhere so that properties like viscosity can be macroscopically averaged irrespective of the underlying discrete molecular structure of the fluid.[12] According to this continuum mechanics view, viscosity can be thought of as resistance to bulk flow of a fluid. From a molecular point of view, in a simple liquid, viscosity can be regarded as a transport coefficient that dictates the rate at which momentum is transported by liquid molecules due to velocity gradients in the flow.

From a continuum perspective, the notion of viscosity as resistance to bulk flow can be conceptualized by considering the case of a simple fluid (e.g., water) in a geometry like that shown in Fig. 3(a). The setup consists of a fixed bottom plate and a parallel top plate separated by a gap (H). When the top plate is moved at a steady velocity (V), the applied stress parallel to the fluid, i.e., shear stress, moves the layers of fluid such that their velocity varies linearly

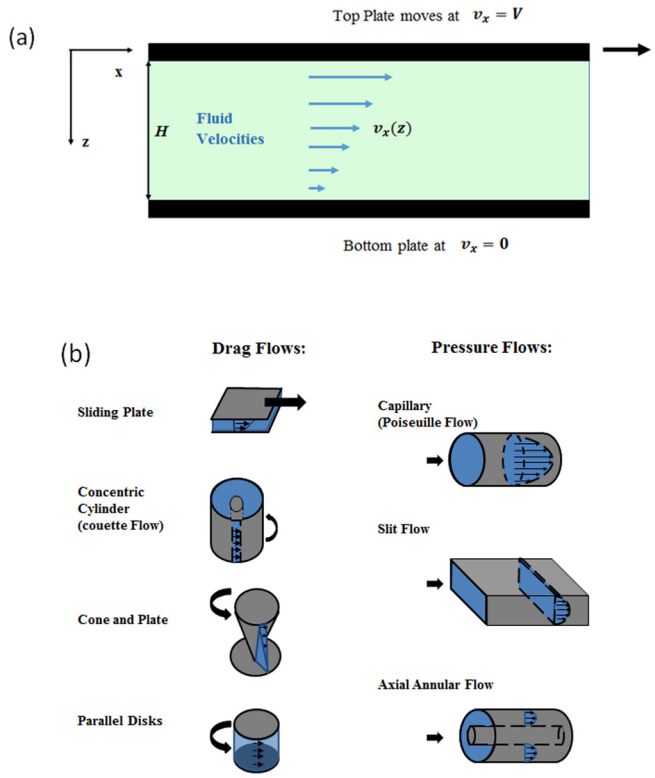


FIG. 3. Shear viscometry and viscometric flows. (a) Shear viscometry of a Newtonian fluid between sliding parallel plates. The top plate is moved at constant velocity while the bottom plate is fixed leading to a homogenous shearing of the Newtonian fluid. (b) Different macroscale geometries used to measure the rheology of complex fluids. The left column shows geometries that generate boundary-driven flows, while the right column shows geometries that create pressure-driven flows. From Macosko, *Principles of Rheology: Measurements and Applications*, Copyright 1994 John Wiley and Sons, Inc., Adapted with permission from John Wiley and Sons, Inc.

throughout the gap as shown in Fig. 3(a). Since there is a relative difference in velocity between the fluid layers, an element of fluid in this setup experiences shear deformation.

It has been found empirically that the shear stress imposed on the fluid is proportional to the rate of shear deformation, with the proportionality constant being viscosity—also called as Newton's law of viscosity. In this case, viscosity dictates the ability of adjacent layers of fluid to resist shear deformation. Alternatively, viscosity can also be regarded as a measure of the friction between the fluid layers, and this friction causes the kinetic energy of the fluid layers to be dissipated as heat energy.

Mathematically, in the case of a homogenous deformation resulting from steady simple shear as shown in Fig. 3(a), the coefficient of viscosity can be used to relate the shear stress and the rate of shear deformation as follows:

$$\tau_{zx} = \mu\dot{\gamma} = \mu\frac{dv_x}{dz}, \tag{1}$$

where $\tau_{zx}$ is the shear stress (with the subscript $z$ denoting the direction of the normal vector to the fluid layers and $x$ is the direction in which force is being applied; the sign convention for stress is based on that discussed in Ref. 14), $\mu$ is the viscosity, and $\dot{\gamma}$ denotes the shear rate, which is given by the velocity gradient, $\frac{dv_x}{dz}$. Since the velocity varies linearly within the gap, the shear rate is constant in the fluid. Thus, this setup produces a homogeneous shear flow, where every fluid element experiences the same rate of shear deformation.

The setup shown in Fig. 3(a) also forms a convenient means to measure the viscosity of the fluid. If the force, F, required to maintain the top plate at a constant velocity is known, then

the imposed shear stress is $\tau_{zx} = \frac{F}{A}$, where A is the surface area of the plate. Likewise, since the velocity profile is linear, the shear rate is given by V/H. Thus, using the Newton's law of viscosity (Eq. (1)), one can determine the viscosity of the fluid. Fluids that exhibit a linear relationship between shear stress and shear rate and which do not show elastic response are referred to as Newtonian fluids; otherwise they are non-Newtonian fluids—which is the case for most real world fluids.

The above analysis illustrates a crucial aspect of shear viscometry, which is that the rheological properties of a complex fluid are easiest to determine and interpret when the imposed flow field is simple and readily quantifiable. In the general case of an arbitrary flow field, the one-dimensional form of Eq. (1) is transformed into a tensorial representation given by

$$\underline{\underline{\tau}} = 2\mu\underline{\underline{\dot{\gamma}}} = \mu(\underline{\nabla v} + (\underline{\nabla v})^T), \tag{2}$$

where $\underline{\underline{\tau}}$ is the shear stress tensor, $\underline{\underline{\dot{\gamma}}}$ is the rate of deformation tensor, and $\underline{\nabla v}$ is the velocity gradient tensor (the superscript $T$ denotes transpose). Eq. (2) is a constitutive relation for a Newtonian fluid, connecting the different components of shear stress to their corresponding components of velocity gradients.

For complex fluids, Eq. (2) does not hold, and no unique constitutive relation exists, making it difficult to readily compute rheological properties. Moreover, the rheology of complex- and bio-fluids depends on the imposed flow field or kinematics. To overcome this difficulty, the standard rheological approach is to subject a complex fluid to shear deformation, similar to Fig. 3(a) and calculate an apparent shear viscosity as

$$\mu(\dot{\gamma}) = \frac{\tau}{\dot{\gamma}}, \tag{3}$$

where $\mu(\dot{\gamma})$ is the shear-rate-dependent viscosity of complex fluids. In addition to the simple shear geometry of Fig. 3(a), other geometries are used to characterize the shear rheology of complex fluids (see Fig. 3(b)). These viscometric geometries provide well-defined flow kinematics, allowing closed-form analytical functions for the rate of deformation tensor. In standard rheometry employing these viscometric flows, a crucial assumption is that the flow kinematics resulting from shearing a complex fluid is same as that when a Newtonian fluid is sheared. Although this assumption is not necessarily correct, this approach is practically useful to classify different complex fluids based on their rheological behaviors—e.g., shear thinning or thickening fluids—and forms a test bed for developing continuum and molecular models of complex fluid rheology.[15,16]

## III. LIMITATIONS OF MACROSCALE SHEAR VISCOMETRY

A wide range of approaches exist to characterize the rheology of complex fluids at the macroscale. Briefly, as shown in Fig. 3(b), rheometers based on both drag flows and pressure driven flows are well developed. In drag flow rheometers such as Couette, cone-and-plate, and parallel plate geometries, a moving surface shears the sample. In contrast, a constant pressure drop is imposed in the pressure flow rheometers. Since detailed discussion of the working principles of these macroscale rheometers is given in textbooks by Macoscko[11] and Morrison,[5] here we focus on their limitations in the context of microfluidic steady shear viscometry. A more complete description of the challenges of macroscale rheometry and how to avoid bad data with these methods has been given by Ewoldt *et al.*[17]

### A. Low-viscosity fluids

Measurement of shear rheology over a broad range of shear rates for water-like fluids such as dilute polymer solutions,[18] bacterial fluids,[19] and microalgae suspensions[20] is challenging with macroscale rheometry. The limitation arises due to the lowest torque that can be reliably measured. This particularly affects acquisition of shear viscosity data at low shear rates. Data

can be potentially acquired at higher shear rates, but then secondary flow and inertial instabilities might kick in, limiting the range of reliable data.

### B. Small sample volumes

The amount of sample available for most synthetic complex fluids is large enough that standard rheometric methods can be used for shear rheology characterization. However, this is not the case for many biofluids including monoclonal antibody solutions, DNA solutions, saliva, mucus, and exudates. Fluid volumes can also be a limitation when a diverse set of assays needs to be conducted with the same sample. Thus, macroscale rheometers are incapable of measuring rheology of microliter sample volumes, unless the geometric gaps are scaled down tremendously (which has their own issues as discussed below).

### C. Inertial and secondary flows

The viscometric flows that are employed in macroscale rheometry are prone to inertial instabilities and secondary flows.[21] As a result, it is difficult to obtain shear viscosity data at high shear rates ($>1000\,s^{-1}$). However, viscosity data at very high shear rates ($>10\,000\,s^{-1}$) are important for a range of applications (see Fig. 2(a)) including lubricants and inkjet printing. Nevertheless, very high shear rates ($\sim 10^6\,s^{-1}$) have been achieved by reducing the gaps in viscometric geometries down to the micron-scale,[22–24] but such approaches are complex and require significant technical ingenuity.

### D. Interfacial artifacts

When the sample is placed in a cone and plate, Couette and parallel-plate rheometers, a free interface is inherently present. The presence of this interface can produce artifacts in the rheology data. The artifacts arise due to surface tension forces, evaporation of sample, and film formation by surface-active species. These artifacts are particularly problematic with low-viscosity fluids, where they can mask the fluid's true shear rheology.[25]

### E. Small-gap errors

In some instances, there is a need to conduct rheometry in small gaps, for example, to minimize sample volume, study confinement effects on rheological behavior, or achieve high shear rates. In such cases, parallel-plate geometries are convenient to use. The main challenge then is to ensure uniformity of the gap so that artifacts can be avoided.

In summary, although macroscale rheometers (especially drag-flow rheometers) are powerful in that they can be used to perform a wide range of rheological tests (oscillatory shear, creep, etc.), they have certain limitations associated with steady shear rheometry. As we discuss below, microfluidics is paving the way to address these limitations of conventional rheometry.

## IV. SIGNIFICANCE OF MICROFLUIDICS FOR RHEOLOGY

The science and engineering of manipulating fluids in micron-scale devices has witnessed tremendous growth in the last two decades.[26–29] These advances have opened new opportunities for investigating the flow behavior and characterizing the rheological properties of complex fluids and biofluids. Below, we discuss the main drivers for this significant interest in using microfluidics for rheometry. Some of these drivers parallel the need to address the technical limitations of macroscale rheometry (discussed above), while others are motivated by new fundamental insights.

### A. Small length scales and geometric confinement

The mesoscale structure of complex fluids influences their flow behavior and rheological properties.[30] The length scales associated with this mesostructure in complex fluids range from nanometers (e.g., in protein and polymer solutions) to microns (e.g., in colloidal suspensions

and foams). The scaling down of geometric features also enables confinement of deformable particles such as drops, bubbles, polymer chains, and biological cells. The interaction of fluid forces and these deformable particles under geometric confinement can produce interesting rheological behaviors that are yet to be fully explored. Understanding the rheology of complex fluids at these small length scales is not only fundamentally rich[31] but also important for a wide range of applications including porous media flows[32] and blood flow in capillaries.[33]

Rapid advances in microfabrication methods have provided opportunities to engineer microfluidic devices at a length scale that is compatible with the mesoscale structure of complex fluids. These microfabrication methods have enabled the construction of micrometer-scale channels and features in a variety of materials such as thermosets, thermoplastics, glass, and silicon. The ability to precisely control the flow geometry has led to devices that can measure shear and extensional fluid rheology. In particular, the simplicity and rapid prototyping offered by methods such as polydimethyl(siloxane) (PDMS)-based soft lithography has allowed the widespread adoption of microfluidic devices for probing complex fluids and their rheology at a wide range of length scales.

### B. Access to unique flow regimes

From a viscometry perspective, the small length scales typical of microfluidics provide a convenient means to operate in unique flow regimes, which are difficult to access in macroscale geometries.[29] For example, the Reynolds number defined as $\mathrm{Re} = \rho \mathrm{Vh}/\mu$, where $\rho$ is the fluid density, V is the velocity scale, and h is the smallest characteristic length scale of flow (e.g., channel height), is typically small in microfluidic flows, indicating that viscous forces dominate over inertial forces. Despite the Reynolds number being small, very high shear rates (which scale as V/h) can be achieved, since the characteristic length scale is of the order of microns. Thus, using microfluidic devices, viscosity data can be obtained at high shear rates without crossing over to turbulent regimes. Another dimensionless number of interest is the Peclet number (Pe) which can be used to estimate the extent of diffusional mixing inside microchannels and is given by $\mathrm{Pe} = \mathrm{Vh}/\mathrm{D}$ where D is the molecular diffusivity. High or low values of Peclet numbers can be achieved in microchannels based on channel design and flow rates.

An important consequence of achieving high shear rates is that viscoelastic fluids having small relaxation time can be easily excited in microfluidic flows, and their rheology can be characterized.[18] This is evident from the fact that Weissenberg number ($\mathrm{Wi} = \lambda\dot{\gamma}$ in case of simple shear flow, where $\lambda$ is the relaxation time of the fluid), which is a measure of fluid nonlinearity,[34] is typically high in microscale flows. The ease of accessing the high Weissenberg number regime is well suited for characterizing polymer solution rheology for applications in industrial processes[35] and lubricating flows in oral cavity or synovial joints.[36,37] Similarly, the Deborah number is defined as $\mathrm{De} = \lambda/\mathrm{t_o}$ where $\mathrm{t_o}$ is the time of observation which can be a characteristic of the flow geometry. For example, $\mathrm{t_o}$ could be the residence time for a contraction length (L/V, where L is the length along the contraction), or oscillation time ($\sim\omega^{-1}$) in an oscillatory flow.[29] The Deborah number describes the extent to which the response of a material to a deformation is viscoelastic rather than purely viscous.[34] Microfluidic flows can achieve short observation times and consequently access high values of the Deborah number (De), however, the Reynolds number (Re) remains small due to small channel dimensions. Therefore, large values of elasticity number $\mathrm{El} = \mathrm{De}/\mathrm{Re} = \lambda\mu/\rho\mathrm{h}^2$ can be accessed such that $\mathrm{El} \gg 1$ compared to macroscopic flows where $\mathrm{El} \ll 1$. For these reasons, microfluidics is ideal for studying viscoelastic flows with high elasticity numbers.[38,39]

### C. Characterization of flow and microstructure

Investigating the rheology of complex fluids and biofluids requires that simple deformation fields are imposed, and the corresponding stresses are measured. Given the complex rheological behavior of these fluids, it is often necessary to measure the flow kinematics in the geometry due to effects such as physical wall slip[40] and shear banding.[41] As a result, characterization of the deformation field is a crucial aspect of rheological investigations. In addition to gaining

insight into structural changes in the fluids, it is often useful to integrate techniques such as birefringence and light scattering into rheometric setups.[42] However, it can be challenging to integrate such techniques into bulky rheometry devices, although some of these integrated setups are now available commercially.

The small footprint of the devices and the ability to make them in optically transparent materials has made them a natural fit for microscopic visualization of flow and fluid structure, complemented by rheological characterization. For example, several studies have integrated particle-imaging velocimetry and characterized the velocity fields for complex fluid flows in microchannels.[43–45] The advantage of such a microfluidic approach is that local strain rate can be measured even if physical wall slip is present. In addition to flow characterization, studies have also investigated the structure and dynamics of complex fluids and soft particles in microfluidic flows. Specific examples include DNA-stretching dynamics at the single molecule level[46,47] and mapping the deformation of deformable particles such as drops[48] and cells.[49,50] The stress field due to extensional flow of polymer solutions in microfluidic devices has also been measured using optical birefringence.[51] Overall, the powerful capability to simultaneously characterize the rheology and structure of complex fluids is becoming one of the major driving forces for using microfluidic devices rather than macroscale rheometric methods.

### D. Technological benefits

In addition to fundamental advantages of probing material properties—such as accessing unique flow regimes, flow and microstructure visualization—microfluidic approaches also offer several practical benefits. Microfluidic devices offer the benefit of consuming less sample compared to conventional viscometry requirements, which is especially important for biofluids. For example, microfluidic rheological characterization of blood and plasma has been achieved with sub-microliter sample volumes.[52–54]

The notion of lab-on-a-chip where several functionalities can be simultaneously integrated also provides significant opportunities for microfluidic rheology. Using microfluidics, it is possible to control the composition of fluids, allowing combinatorial viscometry.[55,56] For example, microfluidic combinatorial viscometry has been successfully employed for evaluating the intrinsic viscosities of polymer solutions and biofluids by measuring their viscosities over a range of dilutions on a single chip.[57] Likewise, parallelization can be achieved for rheological analysis of multiple samples.[58,59] Additional technological benefits include portability and disposability of devices, allowing point-of-care rheology. Microfluidic approaches to rheology thus offer several practical benefits, and one of the goals of this review is to highlight the degree to which different viscometric methods address these practical benefits.

## V. MICROFLUIDIC SHEAR VISCOMETRY: BASIC PRINCIPLES AND METHODS

In this section, we discuss the different microfluidic viscometers. Unlike macroscale rheometers, which commonly employ boundary-driven flows, most microfluidic viscometers use internal flows. We describe the basic principle underlying each viscometer technique, its methodology, and key results pertaining to the technique. Table I provides a summary of these different viscometers.

### A. Pressure sensing viscometers

Microfluidic viscometers based on pressure sensors involve measuring pressure drop ($\Delta P$) across a straight microchannel for known imposed flow rates (Q), analogous to macroscale slit flow rheometry,[11] as shown in Fig. 4(a). Usually, thin slit microchannels are fabricated, which allow for the measurement of viscosity using the Hagen-Poiseuille equation for one-dimensional flow.[8,60] The governing equation for determining viscosity is given by

$$\mu(\dot{\gamma}_w) = \frac{wd\Delta P}{2l_0(w+d)}\frac{1}{\dot{\gamma}_w}, \tag{4}$$

TABLE I. A summary of different microfluidic viscometers and the operating limits on their viscosity and shear rates. These data were obtained from the experimental results of the respective studies.

| Microfluidic Viscometers | Shear rate range | Viscosity Range |
|---|---|---|
| 1. Pressure sensing[60] | $1–10^6\,s^{-1}$ | $10^{-3}–10\,Pa\,s$ |
| 2. Flow rate sensing[72,73] | $1–10^4\,s^{-1}$ | $\sim10^{-3}–2\,Pa\,s$ |
| 3. Surface tension[77] | $0.5\times10^1–10^3\,s^{-1}$ | $10^{-3}–6\times10^{-1}\,Pa\,s$ |
| 4. Co-flowing streams[58] | $1–10^4\,s^{-1}$ | $10^{-3}–10\,Pa\,s$ |
| 5. Diffusion based[56] | Not applicable | $\sim10^{-3}–10^{-2}\,Pa\,s$ |
| 6. Velocimetry based[44] | $10–10^5\,s^{-1}$ | Limits not established |

where $w$ is the channel width, $d$ is the depth, and $l_0$ is the separation between the two pressure sensors. The imposed wall shear rate for a complex fluid is given by

$$\dot{\gamma}_w = \frac{\dot{\gamma}_a}{3}\left[2+\frac{d(ln\dot{\gamma}_a)}{d(ln\tau_w)}\right]. \tag{5}$$

Here, $\tau_w$ is the wall shear stress determined from the measured pressure drop, and the apparent shear rate $\dot{\gamma}_a$ is given by

$$\dot{\gamma}_a = \frac{6Q}{wd^2}. \tag{6}$$

In Eq. (5), the derivative denotes the slope of apparent shear rate and the wall shear stress on a log-log plot. This derivative represents the Weissenberg–Rabinowitsch–Mooney (WRM) correction for the non-parabolic velocity profile due to flow of the complex fluid in the microchannel. For a Newtonian fluid, this derivative is unity, while for complex fluids it is calculated by fitting the variation of $\ln(\dot{\gamma}_a)$ with respect to $\ln(\tau_w)$ using a first or second order polynomial.[60]

Pressure can be measured in microfluidic channels through three different strategies: (i) embedding flush-mounted pressure transducers on the floor of the microchannel (Fig. 4(a));[60] (ii) sideways tapping into the microchannel;[61] and (iii) mounting an external pressure sensor at the upstream of the microchannel.[62] Among these approaches, the most effective and widely adopted pressure-sensing method consists of flush–mounted capacitive pressure transducers on the floor of the microchannel. Capacitive pressure sensors are preferred due to their low sensitivity to residual packaging stress and temperature variations compared to piezoresistive sensors.[63,64] The capacitive type-pressure sensors can be fabricated using silicon micromachining technology with air gaps of the O ($5\,\mu m$) between the electrodes and lateral dimensions less

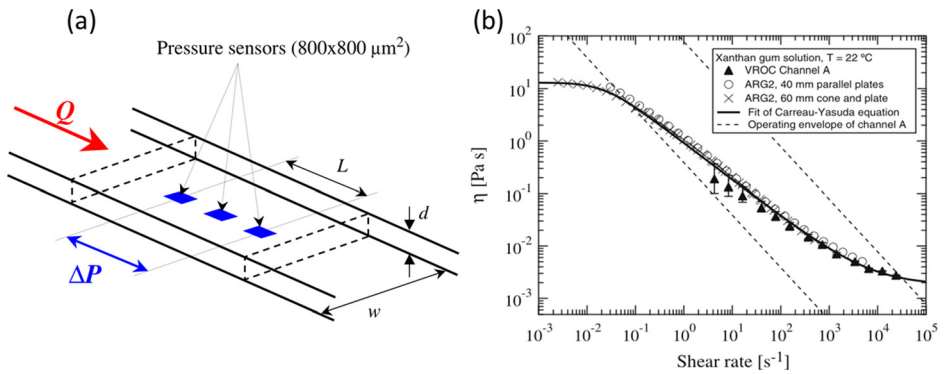


FIG. 4. (a) Pressure sensing microfluidic viscometer with flush mounted pressure sensors. (b) Viscosity as a function of shear rate for aqueous xanthan gum solution showing high shear rate ($10^{-3}–10^4\,s^{-1}$) rheometry with flush mounted sensors. Reproduced with permission from Pipe *et al.*, Rheol. Acta **47**(5–6), 621–642 (2008). Copyright 2008 Springer-Verlag.

than 1 mm. The low gap ensures that pressure measurement is virtually free of any "hole pressure errors" caused by the sensor recessing below the channel floor.[65,66]

In the work of Pipe *et al.*,[60] sensors were mounted inside thin-slit microchannels with widths ($w$) typically between 2 and 3 mm and depths ($d$) $< 100\,\mu$m in order to ensure low aspect ratios ($a = d/w$) $\ll 1$ for the validity of Eq. (4). The pressure sensor array is mounted at a sufficient distance downstream of the inlet to neglect any entrance effects and to ensure fully developed flow.[60] Another variation of this approach was demonstrated by Pan and Arratia[67] where they used roof-mounted deformable membranes integrated with piezoresistive pressure sensors for *in-situ* pressure sensing. Pressure sensing can also be accomplished by means of sideways tapping taken from the main microchannel wall.[61] Such an approach bypasses the issue of "hole pressure errors," because the sensors are located away from the path of direct flow.

Another distinct approach avoids the use of on-chip pressure sensors altogether and consists of pump-mounted pressure transducers which are off-chip. However, in off-chip pressure transduction, the sensor is located away from the main microchannel and measures the overall pressure drop. To calculate the effective pressure drop across the actual microchannel, careful design and analysis considerations are required, such as accounting for end pressure corrections, elongational entrance flow, and large contraction ratios at the ends where the microchannel chip connects to the piping.[62]

Complex as well as Newtonian fluids have been successfully characterized using the flush-mounted pressure sensors over a wide range of viscosities and high shear rates ($\sim 80\,000\,s^{-1}$). This type of pressure-sensing viscometer is commercially available, making it more accessible for researchers (see www.rheosense.com). Pipe and co-workers tested polymer solutions of xanthan gum (Fig. 4(b)), polyethylene oxide (PEO), and worm-like micellar solution of cetylpyridinium chloride/sodium salicylate in sodium chloride brine (CpCl/NaSal) using this approach, and the viscosity data were found to be in good agreement with macroscale rheometry.[60] Al-Roubaie *et al.* measured the shear-thinning viscosity of embryonic avian blood over a wide range of shear rates ($20$–$1000\,s^{-1}$).[68] Sharma *et al.* successfully measured the shear rheology of globular proteins free from interfacial effects.[25] The viscometry of saliva was also investigated by Haward *et al.* using this approach.[69] Additionally, Pan and Arratia used another variant of this approach to measure viscosities of glycerol solutions and xanthan gum.[67] In addition to shear viscosity, the flush-mounted sensors have also been used to measure apparent extensional viscosity in hyperbolic contraction geometries.[70] Alternately, the viscometer design with sideways pressure sensing has been shown to successfully carry out viscometry of nanofluids[61] ($SiO_2$ nanoparticles dispersed in silicon oil or ethanol) for shear rates up to $2.5 \times 10^5\,s^{-1}$.

In the case of externally mounted pressure sensor based viscometers, the highest shear rates that can be accessed were reported to be $10^6\,s^{-1}$. Kang and co-workers used this device for measuring the viscosity of PEO and hydroxyethyl cellulose (HEC) solutions.[62] This type of viscometer is capable of complex fluid viscometry. However, the effect of viscoelasticity on entrance lengths is not known with accuracy, which can affect the final measurement.

The simplicity and commercial availability of on-chip pressure-sensing viscometers make them good candidates for low sample volume ($>20\,\mu$l depending on viscosity) shear viscometry of complex fluids. They are particularly well suited for high shear rate ($\sim 0.5$–$1\,400\,000\,s^{-1}$) viscosity measurements, and their portability makes them suitable for point-of-care rheology applications.[71] However, in the case of low viscosity fluids O ($10^{-3}$ Pa s) the sample volume required can run as high as 15 ml in order to achieve suitable pressure drops and shear rates.[60] Moreover, the error reported with the flush mounted pressure sensing device at the lowest shear rates O ($10\,s^{-1}$) can be large O ($\pm 50\%$) due to the sensitivity of the transducer. Finally, due to active contact of the fluid with the on-chip pressure sensor, these devices are not disposable and necessitate washing protocols, especially if biofluids or particulate fluids are being used.

### B. Flow rate sensing viscometers

At the macroscale, stress-controlled or strain-controlled rheometers exist, depending on whether stress or strain is the control parameter. Analogously, in microfluidic viscometry,

pressure-sensing viscometers can be regarded as strain-controlled where the rate of deformation is controlled, while flow rate sensing viscometers are stress-controlled where the driving pressure is the control parameter.

In practice, flow rate sensing viscometers have a similar working principle as pressure sensing microfluidic viscometers; instead of measuring the pressure drop, however, the flow rate is measured, and Eq. (4) is used to determine the shear viscosity. The shear rate is also determined in a similar manner as pressure sensing viscometers (see Eqs. (5) and (6)).

Two different methodologies for measuring viscosity based on flow-rate measurement have been reported so far.[72,73] Hudson *et al*. demonstrated flow rate sensing viscometry by essentially miniaturizing capillary viscometry to handle microliter-volume samples. The implementation strategy involved pressure chambers with an internal flow path in the form of a cylindrical capillary combined with an in-line commercially available flow meter for measuring flow rate (Fig. 5(a)). To eliminate the air-liquid interface, which can create problems for protein solution rheology, the connecting tubing was initially filled with water. Conditions were optimized such that the miscible displacement front and dispersion did not dilute the sample. The resistance of the entire flow path was taken into account by calibrating with a fluid of known viscosity.

As shown in Fig. 5(a), the micro-capillary rheometer of Hudson *et al*. was able to estimate the viscosities of monoclonal antibody (mAb) solutions at different combinations of concentration (20–100 g/l) and temperature (5–40 °C). Fig. 5(a) shows the wide range of shear rates over three decades (10–10 000 $s^{-1}$) achieved using this device for antibody solutions over a viscosity range of 0.7–10 mPa s. Moreover, the total volumes consumed for each of these measurements were small ~10 $\mu$l. The measurement of viscosity for antibody solution was compared against the commercially available m-VROC rheometer (see www.rheosense.com), and the results were found to be in good agreement.

In an alternative method, Solomon *et al*. devised a flow rate sensing viscometer called iCapillary.[73] In this method, a fixed pressure is imposed for driving the fluid inside a microchannel (Fig. 5(b)). The flow rate is measured by recording the motion of the air-liquid interface in a larger diameter glass capillary attached to the microchannel. The device was designed such that the pressure drop mostly occurs across the microchannel, and the contributions from the attached glass capillary and the Laplace pressure across the air-liquid interface are small (<5%). A smart-phone

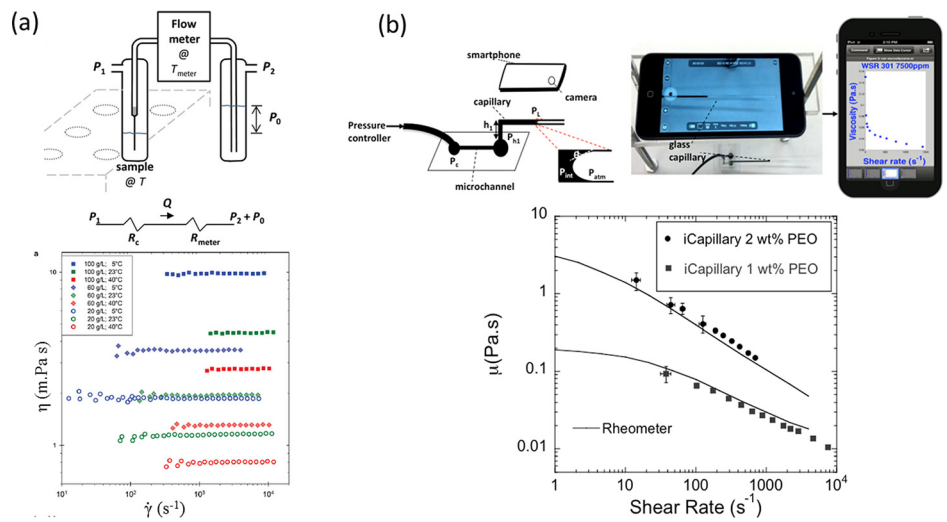


FIG. 5. Flow rate sensing viscometers. (a) (top) Schematic of the pressure-driven micro-capillary rheometer showing the two pressure chambers connected by polyethylene tubing along with the circuit diagram showing resistance of the flow path. (bottom) Measured viscosity of different concentrations (20–100 g/l) of antibody solutions over a range of shear rates at pH 8.7 and temperatures of 5 °C, 23 °C, and 40 °C, showing Newtonian behavior. Reproduced with permission from Hudson *et al*., J. Pharm. Sci. **104** (2), 678–685 (2015). Copyright 2015 Elsevier. (b) (top) iCapillary viscometer setup and operation. (bottom) Viscosity values of 2 wt. % (circles) and 1 wt. % (squares) PEO solutions obtained using the iCapillary device. The lines are data from macroscale rheometry.[73]

camera was used to record videos of the interface motion, thus decoupling the sensing element and flow path, enabling disposable devices for viscosity measurement.

The iCapillary viscometer shown in Fig. 5(b) was used to measure the viscosity of PEO solutions over a wide range of shear rates (10–10 000 $s^{-1}$). In order to generate the viscosity vs. shear rate in Fig. 5(b), about 1 ml of sample was required along with 20 min of experimental time. Since the field of view allowed monitoring of interface motion in multiple capillaries, parallel analysis of bovine serum albumin solutions (BSA; concentration: 5–250 mg/ml) was demonstrated. The rheology data of protein solutions were found to be in good agreement with literature data and models of suspension rheology.[73]

The flow rate sensing viscometers offer a complementary methodology to pressure sensing viscometers but with some distinct advantages. For example, dead volumes and data acquisition time can be minimized with flow rate sensing viscometers, since pressure-sensing viscometers rely on syringe pumps, which inherently have dead volumes and require pump stabilization time between flow-rate changes. In addition, flow rate sensing viscometers are more adaptable to parallel analysis of samples, since it is easier to have distributed pressure sources. A potential disadvantage of flow rate sensing viscometers is the difficulty in achieving viscosity data at ultra high shear rates (>10 000 $s^{-1}$) due to limited range offered by commercial inline flow rate sensors. A similar issue arises with the iCapillary method due to the inability to track very fast fluid motion with smartphone cameras. Another limitation of flow rate sensing devices is that they require pressure controllers in order to impose a fixed pressure drop which introduces the need for additional instrumentation as compared to other simpler techniques, such as the surface-tension based viscometers which are discussed in Sec. V C.

### C. Surface-tension viscometers

The forces of surface tension have been exploited in microfluidic systems to realize passive pumping,[74] enabling check valves[75] and the manipulation of droplets.[76] The use of surface tension for pumping presents a unique opportunity whereby fluid flows can be obtained without the need for cumbersome or expensive instrumentation. In contrast to pressure sensing and flow rate sensing viscometers, surface tension viscometers rely on capillary pressure and wetting properties of surfaces to passively draw fluids into microchannels. The imbibition front of the liquid interface is tracked over time (Fig. 6(a)), enabling determination of viscosity and shear rate. Since the liquid interface velocity varies with time, a single experiment can access a range of viscosities and shear rates.

The viscosity is obtained by analyzing the flow using the Hagen-Poiseuille law. For Newtonian fluids, the viscosity is given by

$$\mu = \frac{d^2}{S}\frac{\Delta P}{v(t)L(t)}. \tag{7}$$

Here, $v$ is the time dependent velocity of the travelling front, $d$ is the depth of the channel, $L(t)$ is the instantaneous length of the liquid column inside the channel, $\Delta P$ is the pressure difference across the liquid column inside the channel, and $S$ is a constant specific to channel geometry. The capillary pressure, ΔP, is given by

$$\Delta P = 2\sigma\cos\theta\left(\frac{1}{d}+\frac{1}{w}\right). \tag{8}$$

Here, $\theta$ is the contact angle, $\sigma$ is the surface tension of the liquid, and w is the width of the channel. For complex fluids that display power law rheology, Srivastava and Burns[77] showed that

$$\frac{1}{L(t)} = C.v(t)^n. \tag{9}$$

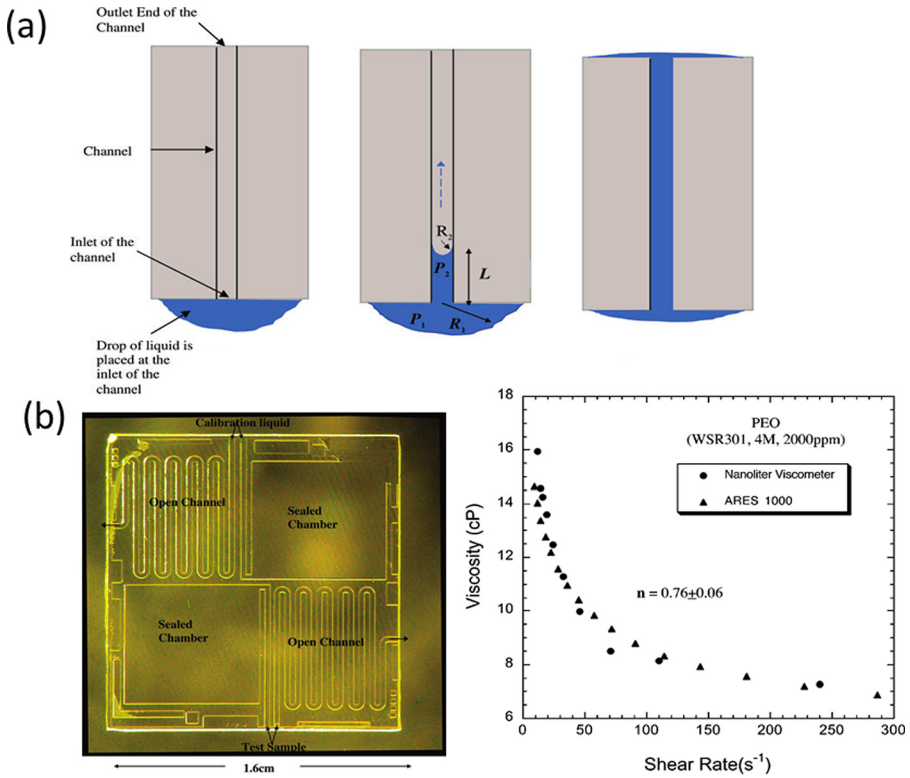


FIG. 6. Surface-tension viscometer. (a) Basic principle of capillary-pressure-driven flow inside microchannels. A drop of liquid placed at the inlet of channel migrates into the channel due to capillary pressure difference between the advancing and receding menisci until it reaches the other end where pressure equalization stops the flow. Reproduced with permission from Srivastava *et al.*, Anal. Chem. **77**(2), 383–392 (2005). Copyright 2005 American Chemical Society. (b) (left) Self-calibrating nanoliter viscometer device with two open channels and two sealed square chambers. (right) Graph showing viscosity as a function of shear rate for a semi dilute solution of PEO at 23 °C, where measurements from a nanoliter viscometer and a cone-and-plate viscometer are compared. Reproduced with permission from Srivastava and Burns, Anal. Chem. **78**(5), 1690–1696 (2006). Copyright 2006 American Chemical Society. Reproduced with permission from Srivastava *et al.*, Anal. Chem. **77**(2), 383–392 (2005). Copyright 2005 American Chemical Society.

Here, $n$ denotes the power law index and $C$ is a constant. A log-log plot of $1/L$ vs. $v$ can be used to estimate the power law index "n." Using this power-law index, the viscosity for a power law fluid can be calculated as

$$\mu = \frac{d^2}{S}\frac{1}{\left(\frac{2}{3}+\frac{1}{3n}\right)}\frac{\Delta P}{v(t)L(t)}. \tag{10}$$

The shear rate for power law fluids is given by

$$\dot{\gamma}_w = \frac{6v(t)}{d}\left(\frac{2}{3}+\frac{1}{3n}\right). \tag{11}$$

Microfluidic surface tension viscometers are relatively simple in that they consist of a long microchannel for measuring the dynamic velocity and length of a traveling liquid column (Fig. 6(b)). The material of the device is an important parameter as it dictates the wettability to the fluid of interest (e.g., a glass substrate bonded to a silicon wafer was used to test aqueous fluids[52]). The operation is relatively simple and does not require active or moving parts. A drop of the fluid is placed at the inlet of the device and is drawn inside due to surface tension (Fig. 6(a)). The growth of the liquid column inside the microchannel is quantified using video imaging or on-chip electrodes.[78]

In this method, two parameters, the geometric factor $d^2/S$ and the driving pressure drop ($\Delta$P), are critical for the viscosity measurement. Srivastava *et al.*[52] introduced a self-calibrating functionality on their device to determine both of these factors. As shown in Fig. 6(b), two sealed and two open chambers are fabricated on the chip for use with a test and a standard calibrating fluid. To determine the geometric factor $d^2/S$, a calibrating fluid (e.g., water) is placed at the inlet of the open channel as well as the sealed chamber. The volume of the air column displaced by the calibrating fluid as it travels into the sealed chamber provides an accurate estimate of pressure drop (through the ideal gas law). The geometrical factor is obtained by observing the velocity through the open channel (in conjunction with the pressure drop and viscosity, see Eq. (7)). Similarly, the capillary pressure for the test fluid can be obtained by placing a drop at the inlet of the sealed chamber. Armed with the knowledge of the geometric factor for the open channel and the capillary pressure from the sealed chamber, the viscosity of the test fluid can be obtained. The actual calculation for the viscosity of the test fluid is done by writing Eq. (7) or Eq. (10) for Newtonian or complex test fluids, respectively, and the calibrating fluid, then taking the respective ratio of the test fluid viscosity and the calibrating fluid. This method provides robust self-calibration functionality.

Microfluidic surface tension viscometers consume extremely low sample volume ($\sim$0.6 $\mu$l) and have been shown to measure the rheology of complex fluids such as blood plasma, PEO solutions (Fig. 6(b)), xanthan gum, and polyacrylamide solutions (PAA). The measured viscosities and shear rates of these various fluids ranged from 1–600 cP and 5–1000 $s^{-1}$, respectively.[77] Thus, this class of viscometers is successfully able to conduct complex fluid viscometry and has significant potential as point-of-use devices due to their extremely small footprint.[52,78]

One of the major advantages of the surface tension viscometer is that it does not require any moving parts and is operationally simple unlike most microfluidic viscometers. In addition, these viscometers are disposable and tend to have quick readout times (<1 min).[52] The limitations of this viscometry technique are wetting defects, inability to access very high shear rates, and complex flow issues due to entrance effects.

### D. Co-flowing stream viscometers

The shear viscosity of complex fluids can be measured by flowing two laminar streams of fluids next to each other typically in a Y-shaped microchannel (Fig. 7(a)). As shown in Fig. 7(a), the basic principle of a co-flowing stream viscometer involves flowing a fluid of known viscosity (reference fluid) adjacent to a fluid of unknown viscosity (test fluid). By recording the location of the fluid-fluid interface between the two streams in the "comparator" region[79,80] for a range of injection flow rates (Q), the viscosity curve for a complex fluid can be determined. In this approach, the governing equation for determining the viscosity is given by

$$\frac{\mu_T}{\mu_R} = \frac{Q_R}{Q_T}\left[f\left(Y, \frac{h}{W}\right)\right]^{-1}, \tag{12}$$

where the subscripts $T$ and $R$ refer to the test and reference fluids, respectively, $Y$ is the interface location ($\left(Y = \frac{1}{2} - \frac{w_R}{W}\right)$, where $\frac{w_R}{W}$ is the fraction of the channel width occupied by reference fluid), and $\frac{h}{W}$ is the channel aspect ratio ($W$ = total width and $h$ = channel height). In Eq. (12), $f$ is a complex function and is provided in Ref. 58. Eq. (12) is applicable for miscible fluids, i.e., interfacial effects between the streams are negligible. In the particular case of a two-dimensional microchannel (i.e., 1-dimensional flow) or for a thin slit, $f$ is simply dependent on the width ratio, and Eq. (12) reduces to

$$\frac{\mu_T}{\mu_R} = \frac{w_T Q_R}{w_R Q_T}. \tag{13}$$

The viscosity is obtained by experimentally measuring the width ratio and knowing the aspect ratio of the microchannel and the injection flow rates. The mean shear rate experienced

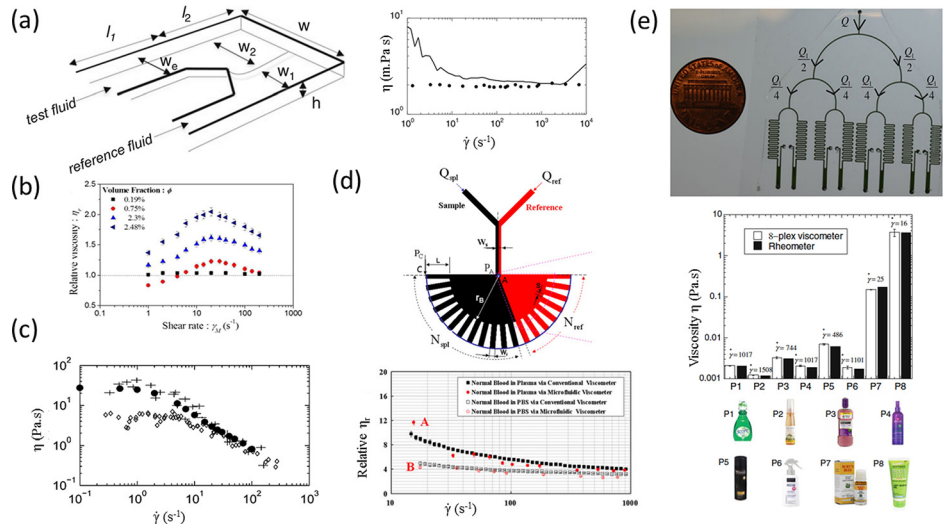


FIG. 7. Co-flowing stream viscometry. (a) Working principle of the comparator-based microfluidic co-flowing streams viscometer and results showing comparison of viscosity as a function of shear rate between rheometer (solid line), and co-flowing streams viscometer using the interface displacement technique (symbols) for a 25 wt. % glycerol solution. Reproduced with permission from Solomon and Vanapalli, Microfluid. Nanofluid. **16**(4), 677–690 (2014). Copyright 2014 Springer-Verlag Berlin Heidelberg. (b) Relative viscosity versus mean shear rate at several volume fractions for bacterial suspensions of *E. coli*. Reproduced with permission from Gachelin *et al.*, Phys. Rev. Lett. **110**(26), 268103 (2013). Copyright 2013 American Physical Society. (c) Viscosity as a function of shear rate for a solution made of 6% CpCl-NaSal in brine water at 22 °C. (◇) represents results obtained in a 200 $\mu$m × 100 $\mu$m glass PDMS channel which are not in agreement with cone plate rheometer at low shear rates. Slip effects on PDMS are at the origin of this deviation. Reproduced with permission from Guillot *et al.*, Langmuir **22**(14), 6438–6445 (2006). Copyright 2006 American Chemical Society. (d) The indicator channel approach showing injected flowrates for sample and reference fluids (Qspl, Qref), and the number of indicating channels filled with the sample and reference fluids (Nspl, Nref). The bottom plot shows comparison of relative viscosity measured by the conventional viscometer and the indicator channel microfluidic viscometer for normal blood—plasma and normal blood–PBS (Phosphate buffered saline) suspension with respect to shear rate. Reproduced with permission from Kang and Yang, Microfluid. Nanofluid. **14**(3–4), 657–668 (2013). Copyright 2013 Springer-Verlag Berlin Heidelberg. (e) The 8-plex co-flowing streams viscometer. Viscosity of various consumer products measured simultaneously using the 8-plex viscometer (open bars). The products are mouthwash (P1, P3), facial spray (P2), hair spray (P4, P5, P6), acne solution (P7), and hair gel (P8). The solid bars represent viscosity data obtained from the rheometer. $\dot{\gamma}$ represents the shear rate at which the data were collected. Reproduced with permission from Solomon and Vanapalli, Microfluid. Nanofluid. **16**(4), 677–690 (2014). Copyright 2014 Springer-Verlag Berlin Heidelberg.

by the test fluid in this approach is evaluated using the following expression for any aspect ratio:

$$\dot{\gamma}_{T,mean} = \frac{1}{w_T h}\int_0^h \int_0^{w_T} \left( \left(\frac{\partial v_x}{\partial y}\right)^2 + \left(\frac{\partial v_x}{\partial z}\right)^2 \right)^{1/2} \partial y \partial z, \tag{14}$$

where $v_x$ is the velocity in the flow direction and $y$, $z$ are transverse directions to the flow. For the case of a low aspect ratio or thin-slit channel, the mean shear rate can be written as

$$\dot{\gamma}_{T,mean} = \frac{3Q_T}{h^2 w_T}. \tag{15}$$

For the case of miscible co-flowing streams, two main approaches exist to implement this technique. In the *interface compensation* method, the flow rates are adjusted to balance the interface, i.e., $\frac{w_T}{w_R} = 1$ or $Y = 0$; and either Eqs. (12) or (13) is used depending on the aspect ratio. In the *interface displacement* method, the interface is allowed to freely adjust (i.e., $-1/2 < Y < 1/2$) for the given flow rates, and the width ratio is measured.

Since miscible fluids are most commonly used in this approach,[58,81] diffusional smearing of the interface needs to be mitigated to accurately quantify the width ratio. As a result, the

method works best when the operating conditions are such that the system is dominated by convection, i.e., Pe $\gg$ 1. Alternatively, diffusion across the interface can be eliminated by using immiscible co-flowing streams, as demonstrated by Guillot *et al.*[82] Given that the normal stress balance is affected by the presence of a curved immiscible interface with interfacial tension, they implemented a numerical procedure to calculate the viscosity of the test fluids from flow rates and measured width values. Although immiscible fluids eliminate interface smearing, a potential drawback of this strategy is that under certain operating conditions, droplets may be formed instead of co-flowing laminar streams.[82]

In most studies, the comparator region consists of a wide rectangular chamber. Kang *et al.*[53,83,84] modified the comparator region by including a number of bifurcating indicator channels in order to directly estimate the occupied widths by the co-flowing streams (Fig. 7(d)). The relative viscosity ($\mu_r$) is calculated from the flow rate ratios and the number of indicator channels ($N$) occupied by each fluid and is given by

$$\mu_r = \left(\frac{\mu_T}{\mu_R}\right) = \left(\frac{N_T}{N_R}\right)\left(\frac{Q_R}{Q_T}\right). \tag{16}$$

Another variation of the co-flowing stream viscometer is to use off-the-shelf cylindrical capillaries rather than lithographically fabricated devices, where a stable liquid/liquid axial annular flow is realized.[85] This method has only been tested for Newtonian fluids and can be prone to hydrodynamic instabilities with elastic fluids.[86]

Co-flowing stream viscometers have been used to measure the shear rheology of a variety of complex fluids across a wide range of shear rates. Guillot and co-workers used the interface displacement mode and tested various Newtonian fluids (water, silicone oil, hexadecane) as well as complex fluid solutions of CpCl/NaSal in brine water (Fig. 7(c)), PEO and PAA. Using this approach they were able to study viscosities of 2 mPa s–70 Pa s (Ref. 82) and access a shear rate range of 0.2–2000 $s^{-1}$. They also automated their viscometry measurements using pump programming, which resulted in sample consumptions lower than 250 $\mu$l for measurements of viscosity as a function of shear rate.[87] Lee and Tripathi[57] used a similar approach to calculate the intrinsic viscosities of polymer solutions of poly(ethyleneglycol), BSA and DNA fragments. Their viscometer was based on diffusional mixing between co-flowing laminar streams and was able to measure viscosity over a range of concentration through on chip dilution. Solomon and Vanapalli parallelized this method to simultaneously measure the viscosity of 8 samples (Fig. 7(e)).[58] In addition to Newtonian fluids, PEO solutions and consumer products (e.g., facial spray and hair gels) were tested across a shear rate range of 1–1000 $s^{-1}$. Choi and Park used the interface compensation mode and measured the viscosity of bovine serum albumin solutions and related it to conformational change of proteins in microflows.[88]

A particular advantage of the co-flowing streams viscometry is that it is well suited for very low-viscosity fluids. As shown in Fig. 7(a), the viscosity of a 2 mPa s glycerol solution can be reliably measured over a wide range of shear rates, which is difficult to achieve on a rotational rheometer. In addition, active biofluids such as bacterial suspensions of very low viscosity have also been characterized with such viscometry. Gachelin *et al.*[19] measured the viscosity of bacterial suspensions and showed the rheo-thinning and rheo-thickening regions of bacterial suspensions (Fig. 7(b)). They also showed that at small shear rates, the viscosity of bacterial suspensions was actually less than that of the suspending fluid while being able to differentiate the rheology of bacterial suspensions varying in volume fraction by as low as 0.2%. Other biofluids such as blood have also been measured with this approach. Kang and co-workers[53] used the indicator-channel-based comparator design (Fig. 7(d)) and measured the viscosity of blood[83,84] over almost one decade of shear rate variation ($\sim$10 $s^{-1}$ to 1000 $s^{-1}$) (Fig. 7(d)).

Instead of a viscometer, the co-flowing stream method can also be configured as a manometer to measure the pressure drop due to flow of complex fluids or confined deformable particles. This manometer approach has been applied to polymer-induced elastic instabilities,[80] flow of confined deformable particles,[89,90] and biological cells.[91,92]

In summary, the co-flowing stream viscometers have been extensively developed and applied to a wide range of complex fluids. Major benefits of this method include the simplicity of the microfluidic geometry design,[93] off-chip image-based measurement, sensitivity to water-like viscosity fluids or samples with small viscosity contrast, wide range of shear rates ($1–1000\,s^{-1}$), relatively low sample consumption (~0.1–1.0 ml), disposable devices, and capability to be automated and multiplexed. Limitations of the method include diffusion-induced blurring of the interface (at very low shear rates) and hydrodynamic instabilities that may occur in the comparator region (at very high shear rates).[58]

### E. Diffusion viscometers

The diffusive motion of micron-scale tracer particles (Fig. 8(a)) suspended in a Newtonian fluid can be used to quantify its viscosity using the Stokes-Einstein-Sutherland relation

$$\mu = \frac{k_B T}{6\pi D a}. \tag{17}$$

Here, $a$ is the particle radius, $T$ is the temperature, and $k_B$ is the Boltzmann constant. Two classes of viscometry approaches exist based on whether the probe particle diffusivity is measured in microfluidic flows or under quiescent conditions.

In microfluidic flow-based diffusion viscometers, co-flowing laminar streams are employed[94] (Fig. 8(b)). But, instead of operating at very high Peclet numbers that are typical of co-flowing stream viscometers, the system conditions are such that diffusion is appreciable. The momentum balance and the convection-diffusion transport equations are simultaneously solved and fit to the experimental data of the diffusively blurred interface to quantify the diffusion coefficient.

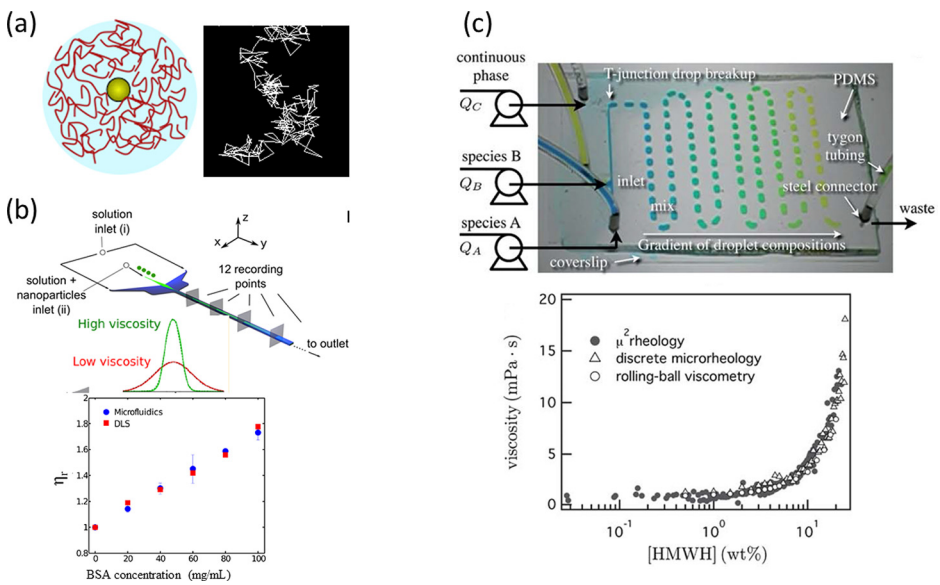


FIG. 8. Diffusion viscometers. (a) Schematic of a particle undergoing Brownian motion in a polymer network. A representative trajectory of the particle is also shown. (b) Flow based diffusional viscometer. Inset shows simulated diffusion profiles for different viscosities. (bottom) Relative viscosity ($\eta_r$) of aqueous solutions at different concentrations of bovine serum albumin (BSA) as measured by flow based diffusional viscometer (circles) and by dynamic light scattering technique (squares) at 25 °C. Reproduced with permission from Arosio *et al.*, Anal. Chem. **88**(7), 3488–3493 (2016). Copyright 2016 American Chemical Society. (c) Droplet based diffusional viscometer. (bottom) Plot showing viscosities of high-molecular weight heparin polymer solutions using high throughput multi-particle tracking rheology in droplets compared with conventional rolling ball viscometry. Reproduced with permission from Schultz and Furst, Lab Chip **11**(22), 3802–3809 (2011). Copyright 2011 The Royal Society of Chemistry.

Flow-based diffusion viscometers have been developed only recently. Arosio *et al.*[94] demonstrated a flow-based microfluidic diffusion viscometer which employed green fluorescent nanoparticles as tracers within a sheathing flow configuration. The analyte solution was introduced in the lateral inlets leading to the main microchannel while the tracer nanoparticles were focused in a narrow beam at the center of the channel (Fig. 8(b)). The nanoparticles diffused laterally with the flow, and images at different downstream locations were collected using a camera attached to a microscope in order to record the diffusional smearing. The measured diffusion profiles of the analyte at a downstream distance were compared to previously generated simulation libraries in order to evaluate the diffusion coefficient, and subsequently viscosity was calculated based on Eq. (17). In these experiments, the typical probe diameter varied from 47 nm for BSA solutions and glycerol mixtures to 100 nm for the crude cell lysate. The concentration of nanoparticles was kept constant at 0.02% in all the experiments. The sample consumption was reported to be around 20–40 $\mu$l of analyte solution and 5–10 $\mu$l of the tracer. Finally, an important operational consideration in these devices is to choose the flow rates such that diffusion is significantly pronounced in order to ensure accurate measurement but not so pronounced that particles reach the channel walls, at which point information on diffusion profiling is lost.

Arosio and co-workers[94] used their flow based diffusional viscometer to estimate the viscosity of BSA at different concentrations (20–100 mg/ml) (Fig. 8(b)) at a flow rate of 40 $\mu$l/h, which corresponds to an apparent wall shear rate of approximately 355 $s^{-1}$ where they are Newtonian. Their result for the viscosity of BSA solution for the 100 mg/ml concentration compares well with another study[25] which investigated interfacial effects on the rheology of globular proteins at similar conditions of shear rate, showing the suitability of this technique for the viscometry of protein solutions. We note that flow-based diffusion viscometers have not been extended to fluids with strong non-Newtonian character.

In contrast to the measurement of tracer diffusivity in microfluidic flows, viscosity can also be determined under quiescent conditions. In this case, the translational motion of probe particles is tracked, and their mean-squared displacement ($\langle x^2 \rangle$) is measured as a function of time. Since for a Newtonian fluid, $\langle x^2 \rangle = \mathrm{nDt}$ (where n is the dimensionality of the measurement), the diffusion coefficient of the probe particle can be determined, and viscosity extracted from Eq. (17) for a Newtonian fluid. The quiescent measurement of tracer diffusion has been extended successfully to complex fluids using the Generalized Stokes-Einstein relation[95] and forms the basis of particle-tracking microrheology methods, which has become a specialized field in itself,[96,97] especially for characterizing the rheology of biofluids.[98,99]

In the quiescent mode of diffusion viscometry, several methodologies exist to measure the diffusion coefficient of probe particles including optical traps,[100–102] image-based multi-particle tracking,[56] dynamic light scattering,[103] and fluorescence correlation spectroscopy.[104] Although these methods have been in existence much longer than microfluidic diffusion viscometers, there has been renewed interest in integrating these techniques into microfluidic formats to harness benefits such as ultra-small sample volumes and multiplexed analysis. For example, recently Schultz and Furst[56] employed droplet-based microfluidics, created samples of different concentration gradations, and measured viscosities using multi-particle tracking based diffusion viscometry (Fig. 8(c)). They successfully measured the viscosities of glycerol solutions (~0–75 wt. %) and high-molecular weight heparin (HMWH) solutions (~0–20 wt. %) (Fig. 8(c)), which were found to be in good agreement with experiments conducted using a conventional rolling-ball viscometer. Additionally, the viscometry with HMWH was able to successfully identify the transition between dilute and semidilute regimes with an estimate of the overlap concentration as $5.9 \pm 1.2\%$, which was in close agreement with a theoretically calculated value of 6.5 wt. %, thus displaying the suitability of this approach for the viscometry of polymers. Compared to conventional falling-ball viscometry, the droplet-based viscometer of Schultz *et al.*, was able to analyze 17-times more samples in 1/6th of the time with a 260-fold reduction in sample consumption.[56] In heterogeneous systems, this approach has the capability to provide local viscosity information.

In summary, flow-based diffusion viscometers and quiescent-condition viscometers offer distinct advantages. They are a convenient means to measure viscosity in the "absence of shear," with the benefits of small sample volumes, parallel analysis and high sensitivity in measurement. They offer a novel way to map viscosity under local variations of temperature, pH, etc., and can be used to further probe the heterogeneities in biological systems. The limitations of diffusion viscometers arise due to difficulty in measuring nonlinear rheology along with the care needed to choose probes of suitable size and chemistry, such that unwanted interactions with the material are avoided.

### F. Velocimetry-based viscometers

Velocimetry-based viscometers rely on measuring the velocity profile for a fluid in a thin-slit microchannel at a given pressure drop (see Fig. 9(a)). Once the flow field inside the microchannel has been obtained (Fig. 9(b)), the local shear rate can be calculated from the gradient of the velocity profile as

$$\dot{\gamma} = \frac{dv_x}{dz}. \tag{18}$$

Here, $v_x$ is the fluid velocity along the direction of the flow and $z$ is local coordinate for the channel height. For a fully developed flow, the *local* shear stress can be related to the imposed pressure gradient as

$$\tau_{zx} = -\frac{\Delta P}{L}(z - z_0). \tag{19}$$

Here, $\Delta P$ is the imposed pressure, $L$ is the length of the microchannel, and $z_0$ denotes a reference position which does not have to coincide with the midplane of the microchannel. For every $\Delta z$ horizontal slice, the local shear rate and shear stress can be calculated using Eqs. (18)

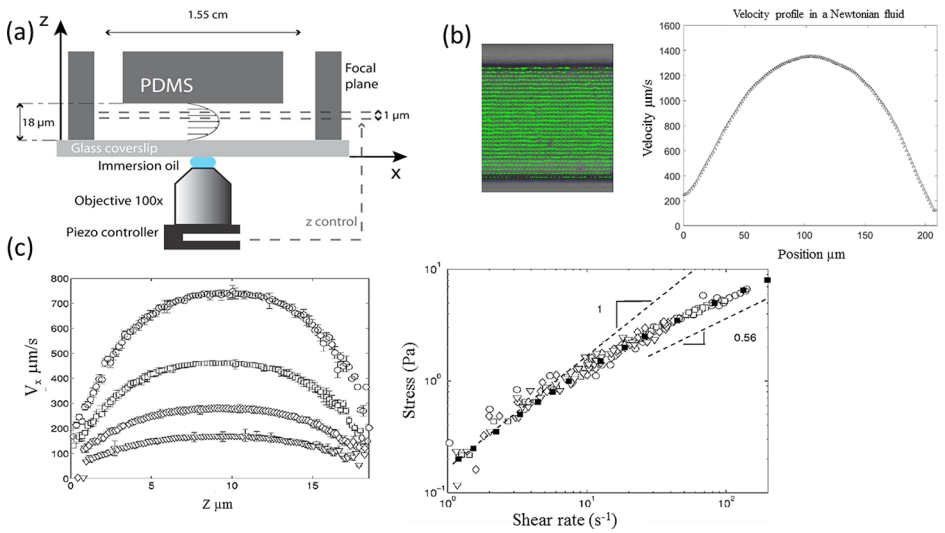


FIG. 9. Velocimetry-based viscometers. (a) Experimental setup for viscometry of complex fluids using particle image velocimetry. Reproduced with permission from Appl. Phys. Lett. **89**(2), 024104 (2006). Copyright 2006 AIP Publishing LLC. (b) (Left) Velocity vector field for flow of a Newtonian fluid in a $200 \times 200\,\text{mm}^2$ (green arrows are in the direction of flow). (Right) The parabolic velocity profile for the corresponding fluid flow (from unpublished data). (c) (Left) Velocity profiles for a PEO solution $M_w = 5 \times 10^6$ g/mol, C = 7.5 g/l at 27 °C for different pressure drops. (○) 122 mbar, (□) 96 mbar, (▽) 71 mbar, and (◇) 52 mbar from a 1.55 cm long and $18 \pm 0.05\,\mu$m thick PDMS on a glass microchannel. Stress vs strain rate curve for the corresponding velocity profiles. (Right) The filled squares are independent measurements performed using a Couette rheometer. The dashed lines are guides for the eyes for slope 1 and 0.56, respectively. Reproduced with permission from Appl. Phys. Lett. **89**(2), 024104 (2006). Copyright 2006 AIP Publishing LLC.

and (19). As a result, a curve of shear stress versus shear rate (see Fig. 9(c)) can be generated, thereby allowing calculation of the shear viscosity curve, since

$$\tau_{zx} = \mu\dot{\gamma}. \tag{20}$$

A unique feature of this approach is that it allows direct measurement of $\tau_{zx}(\dot{\gamma})$ without any a priori assumptions of the fluid or flow field. As a result, WRM correction is not needed, allowing for a much more direct quantification of the shear rheology of the complex fluid. In addition, any effects associated with wall-slip[44] and shear banding[41] are easier to detect with this approach, which are of potential concern when making rheological measurements with complex fluids.

The methodology that is used for this type of viscometry is particle-image velocimetry (PIV), which uses the imaging of probe particles to quantify the flow field. PIV has become a standard method for visualization and characterization of complex flows, including flows in microfluidic devices.[105] The working principle of PIV is to image the motion of tracer particles added to the fluid (Fig. 9(a)). Each image in the acquired video is divided into a uniform grid, where each grid unit is called an interrogation window. The image from an interrogation window at a given time point is statistically compared to its own image at the next time point using a spatial correlation function. This procedure is repeated over all the interrogation windows for visualization of the complete flow field and to provide velocimetry data (Fig. 9(c)).

The key requirements for PIV are that the seeded particles do not significantly alter the original flow field. For complex fluids that are optically clear, bright field imaging can be used; for slightly opaque fluids, epifluorescence microscopy can be used. The material used in making microfluidic devices is also of consideration, since they need to be optically transparent and have little auto-fluorescence. Usually, PDMS-based microfluidic devices suffice for most PIV-based applications.

The first demonstration of a velocimetry-based microfluidic viscometer is by Degre *et al.*[44] As shown in Fig. 9(b), the velocity profiles for a PEO solution at different imposed pressure drops are shown, which are subsequently used to calculate the stress versus shear rate curve. They extended the measurements to different concentrations of PEO solutions and found good agreement with Couette rheometry. Interestingly, they also observed wall slip (see Fig. 9(b) for the case where velocity profile does not extrapolate to zero), but the rheology measurements were insensitive to this issue, as in this method, local shear rates are calculated based on velocity differences and not absolute values. Subsequently, researchers have used this to characterize the rheological behavior of jammed emulsions and soft colloids.[43,45]

PIV-based viscometry of complex fluids is a non-invasive and precise means to characterize the rheology of complex fluids. The approach provides point-wise velocity information enabling direct quantification of shear rate distribution in the flow as well as inspection of any flow heterogeneities. A wide range of shear rates can be accessed based on the geometry of the microchannel, and the technique is amenable to parallel analysis of samples. The technique has limitations with opaque fluids and is somewhat technically demanding with respect to instrumentation and image processing.

### G. Viscosity indexing devices

There are a number of miscellaneous microfluidic approaches that have been reported for measuring viscosity of fluids, with operating principles ranging from electrowetting to droplet deformation and vibrating element-based sensors (see Fig. 10). However, these techniques are limited to Newtonian fluids or provide a qualitative fingerprint for a complex fluid since the deformation fields are non-viscometric.[106] The non-viscometric nature of the flow may arise as a consequence of complicated flow geometries precluding numerical modeling or due to nonlinear rheological response of the fluid. In these methods, in general, the kinematics is such that simple viscous response cannot be isolated from response due to extensional and rotational components of the flow. We review these methods briefly for the sake of completeness.

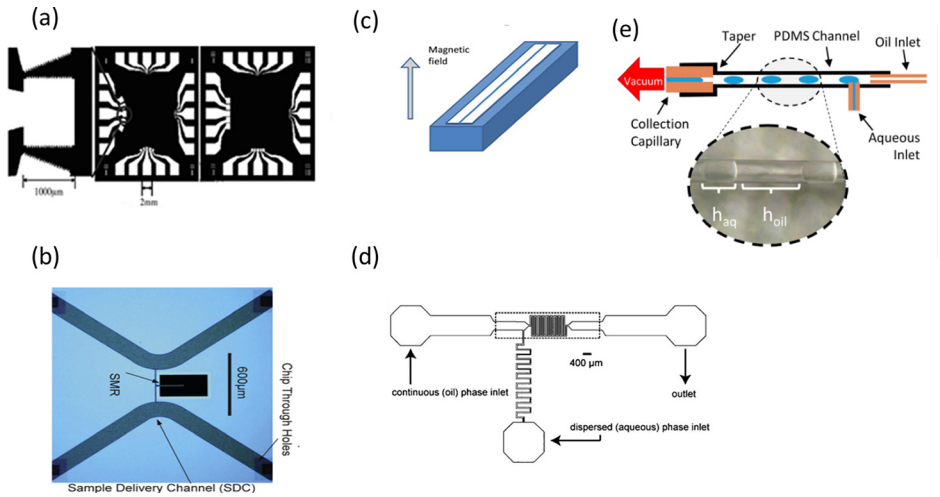


FIG. 10. Microfluidic viscosity indexers (a) Electrowetting viscometer with electrodes. Reproduced with permission from Lin *et al*., Electrochim. Acta **52**(8), 2876–2883 (2007). Copyright 2007 Elsevier. (b) Cantilever based viscometer. Reproduced with permission from Khan *et al*., Sens. Actuators B: Chem. **185**, 456–461 (2013). Copyright 2013 Elsevier. (c) Vibrating nanowire inside a microchannel with applied magnetic field. Reproduced with permission from Rev. Sci. Instrum. **82**(3), 035113 (2011). Copyright 2011 AIP Publishing LLC. (d) Droplet squeezing constriction viscometer. Reproduced with permission from Livak-Dahl *et al*., Lab Chip **13**(2), 297–301 (2013). Copyright 2013 The Royal Society of Chemistry. (e) Droplet based microfluidic viscometer with standard T-junction. Reproduced with permission from DeLaMarre *et al*., Anal. Chem. **87**(9), 4649–4657 (2015). Copyright 2015 American Chemical Society.

### *1. Electrowetting-based viscometer*

Electrowetting based microfluidic viscometry (Fig. 10(a)) is a novel technique in which electrical forces are exerted with the help of embedded electrodes in order to actively drive a liquid droplet inside a microchannel and the viscosity is calculated based on the velocity of the droplet, the channel geometry, and the properties of the dielectric. Electrowetting viscometers currently require high power voltage sources, advanced control systems, and have a low viscosity measurement range however their adoption may increase in future applications due to portability.[107]

### *2. Vibrating element-based viscometer*

Vibrating element based viscometers operate on the principle of a resonating element such as a tuning fork, vibrating wire, or cantilever type oscillator element inside the test fluid. The viscosity can be measured by recording and analyzing the behavior of the oscillating/vibrating element. Khan and co-workers[108] reported a resonance based viscometer (Fig. 10(b)) that is capable of measuring viscosity of samples as low as 5 pL with analysis times of ∼30s. Another type of vibrating wire viscometer by Dehestru *et al*.[109] was reported to be suitable for high pressure (10 psi–24 000 psi) and high temperature (10–200 °C) applications[110] (Fig. 10(c)).

In addition to viscosity, vibrating element-based viscometers are also capable of oscillatory shear rheology providing information on material properties such as the viscous and elastic moduli.[111] Due to the absence of moving parts, vibrating element viscometers require little or no maintenance and can be used in severe operating environments for wide range of fluids including fouling fluids and high-viscosity fluids, however, since they do not have a well-defined shear field they are not suitable for probing complex fluid behavior over a range of shear rates.

### *3. Droplet-based viscometer*

These viscometers rely on the analysis of flow of a sample plug immersed in an outer phase such as oil for calculating viscosity.[112,113] In one approach reported by Livak-Dahl

*et al.*,[112] the sample plug was constricted inside a narrow channel representing 99% of the hydrodynamic resistance of the entire microfluidic channel (Fig. 10(d)). The velocity of the plug interface is recorded to calculate the viscosity of the plug from the Hagen Poiseuille equation. In another method reported by DeLaMarre *et al.*,[113] a standard T-junction combined with a cylindrical channel is used to generate the aqueous sample plug in an immiscible oil phase and viscosity information is encoded in the droplet spacing (Fig. 10(e)).

Droplet based nanoliter viscometers offer the advantage of extremely low sample consumptions and have the potential to be integrated with additional readouts such as absorbance. Microfluidic droplet generation and handling systems are desirable for many laboratory applications such as reagent-handling, reaction, separation, dilution, and assaying operations,[114] which makes droplet based viscometers desirable as integrable lab-on-a-chip components. A disadvantage of this approach is the requirement of using an outer immiscible phase of lower viscosity along with accurate pressure control. Moreover, the applicability of these viscometers is restricted to Newtonian fluids of low viscosity.[112,113]

## VI. CHALLENGES AND FUTURE DIRECTIONS

In this review, we have discussed the significance of microfluidics for shear rheology and contrasted its benefits against macroscale rheometry. We also discussed current methods to conduct shear viscometry with microfluidic devices. Despite their many advantages, microfluidic viscometers have certain limitations such as difficulty in handling fouling fluids[115] and the possibility of channel deformation when flexible construction materials are used such as PDMS.[116,117] In contrast to macroscale rheometers that are capable of performing a variety of rheological measurements to obtain material functions, very little progress has been made in using microfluidic devices to measure material functions other than viscosity.

With regards to determining steady shear viscosity curves, microfluidic viscometers have the potential to replace macroscale pressure-flow rheometers such as capillary, slit flow, and axial annular flow devices (see Fig. 3(b)). The field of microfluidic viscometry is growing, and significant opportunities exist for development of devices with enhanced capabilities. Below, we discuss the different areas where there is scope for improving microfluidic shear viscometry methods.

### A. A continuous and broad range of shear rates

Our survey of literature has shown that current microfluidic viscometers are readily capable of offering shear rates ranging from O (1) $s^{-1}$ to O ($10^6$) $s^{-1}$. However, these shear rates are attained by varying the source flow rates or pressures, which can be tedious, especially when a large range of shear rates is desired. Given the precision control that microfluidics offers in terms of the shape of the bounding walls, it should be possible to "hard-wire" a range of shear rates into the microfluidic geometry itself. These avenues need to be investigated in the future. In addition, a lower shear rate range of $10^{-3}$–1 $s^{-1}$ has not been achieved, even though it is important for determining zero-shear viscosity of complex fluids. The main challenge here is that very low source flow rates or pressures are difficult to achieve, and larger channel heights are not easy to fabricate with photolithography methods. However, with the advent of 3D printing technologies[118] and new interest in millifluidics,[119] perhaps these difficulties can be breached.

### B. Point-of-care rheology

As discussed in the review, several microfluidic approaches are capable of measuring shear viscosity using disposable devices, which can lend themselves to onsite viscometry. These use-and-throw devices offer significant potential for measuring the viscosity of biofluids in disease settings. For example, changes in the rheology of blood, mucus, and synovial fluids have been linked to cardiovascular,[120] pulmonary diseases,[121] and rheumatoid arthritis,[122] respectively. Applications in petroleum and consumer products industries will also benefit from field-portable

devices. These point-of-care applications are also where microfluidic viscosity-indexing devices can play an important role.

### C. High throughput

The throughput of analysis is an important consideration when a large number of samples need to be analyzed for their viscosity in a relatively short period. Such situations do indeed arise in pharmaceutical formulations, biomaterials, and consumer products. To date, few microfluidic viscometry techniques have been shown to be capable of handling multiple samples.[56,58,73] Given that macroscale rheometers are extremely difficult to parallelize, this presents a unique opportunity for microfluidics to play an important role. By combining microfluidic dilution techniques,[123–126] libraries of materials can be potentially screened in a high throughput manner for their rheological properties.

### D. Multifunctionality

Current microfluidic devices for rheological measurements are solely dedicated to deliver a single functionality, i.e., viscosity curves. Given that complex fluids and biofluids show different rheological response based on the deformation field, it is useful to develop microfluidic devices where several rheological responses can be simultaneously measured. For example, is it possible to obtain shear and extensional viscosity by changing the operating conditions or device geometries? Recently, microfluidic devices have been developed to measure the relaxation time of dilute polymer solutions,[127–130] which can be difficult to measure on macroscale rheometers. Integrating measurement of relaxation time of viscoelastic fluids with other rheological properties will make microfluidic rheometers competitive with macroscale rheometers.

### E. Integration of advanced optical techniques

The rheology of complex fluids and biofluids is so rich that incorporation of direct visualization tools to characterize the three dimensional velocity fields and structure during rheological measurements will undoubtedly lead to fundamental discoveries. For example, measurement of velocity profiles due to flow of jammed emulsions in microfluidic shear flows has shown that there is not a universal relation linking local stress and strain rate in the flow.[43] Currently, only PIV methods are well integrated into microfluidic devices to quantify flow curves. Other techniques such as high-speed confocal microscopy,[131] digital holography microscopy,[132] and light sheet microscopy[133] are well positioned to be integrated into the study of flow properties of complex fluids and biofluids. In addition to flow characterization methods, spectroscopic tools can also be potentially integrated into microfluidic rheology experiments.

## VII. CONCLUSIONS

Complex fluids and biofluids are astonishingly diverse. Given that their rheological properties are intimately linked with the underlying microstructure, a major goal of the field has been to explore this connection and uncover fundamental principles that can at least unify certain classes of fluids. In this review, we focused on shear viscosity as one rheological signature of these diverse fluids. We discussed how this quantity can be measured using rheometric methods, and we argued that microfluidic viscometers are transforming microfluidic rheometry into a complementary approach to macroscale rheometry while also addressing their limitations.

We have summarized the latest advances in microfluidic viscometers for the shear rheology of complex fluids and biofluids. Distinct advantages of these miniaturized devices include: low sample volume consumption, ease of inducing geometric confinement, access to high shear rates, and direct quantification of flow fields and fluid structure. As discussed in Sec. VI, there is significant room for opening new vistas in microfluidic rheometry. Building on these current and future advances, we expect that the impact of microfluidic rheology will range from better understanding of complex fluid processing to uncovering structure-property relations to

development of constitutive models to unraveling mechanisms regulating the collective motion of living biofluids.

## ACKNOWLEDGMENTS

This work was partially supported by NSF CAREER (Grant No. 1150836). We thank Naureen Suteria for critical reading of the manuscript. We are grateful to the referees for their insightful comments, which helped to improve the manuscript significantly.

[1]R. G. Larson, *The Structure and Rheology of Complex Fluids* (Oxford University Press, New York, 1999).
[2]D. J. McClements, *Food Emulsions: Principles, Practices, and Techniques* (CRC press, 2015).
[3]S. E. Spagnolie, *Complex Fluids in Biological Systems* (Springer New York Heidelberg Dordrecht London, 2015).
[4]J. N. Wilking, T. E. Angelini, A. Seminara, M. P. Brenner, and D. A. Weitz, MRS Bull. **36**(05), 385–391 (2011).
[5]F. A. Morrison, *Understanding Rheology* (Oxford University Press, USA, 2001).
[6]Ralph H. Colby, J. Rheol. **57**(4), 1047–1055 (2013).
[7]H. H. Lipowsky, Microcirculation **12**(1), 5–15 (2005).
[8]C. J. Pipe and G. H. McKinley, Mech. Res. Commun. **36**(1), 110–120 (2009).
[9]F. J. Galindo-Rosales, M. Alves, and M. Oliveira, Microfluid. Nanofluid. **14**(1–2), 1–19 (2013).
[10]S. Haward, Biomicrofluidics **10**(4), 043401 (2016).
[11]C. Macosko, *Principles of Rheology: Measurements and Applications* (John Wiley and Sons, 1994).
[12]F. A. Morrison, *An Introduction to Fluid Mechanics* (Cambridge University Press, 2013).
[13]H. A. Barnes, J. F. Hutton, and K. Walters, *An Introduction to Rheology* (Elsevier, 1989).
[14]W. M. Deen, *Analysis of Transport Phenomena*, Topics in Chemical Engineering (Oxford University Press, New York, 1998).
[15]R. B. Bird, R. C. Armstrong, O. Hassager, and C. F. Curtiss, *Dynamics of Polymeric Liquids* (Wiley, New York, 1977).
[16]R. G. Larson, *Constitutive Equations for Polymer Melts and Solutions*, Butterworths Series in Chemical Engineering (Butterworth-Heinemann, 2013).
[17]R. H. Ewoldt, M. T. Johnston, and L. M. Caretta, in *Complex Fluids in Biological Systems*, edited by S. E. Spagnolie (Springer, 2015), pp. 207–241.
[18]L. E. Rodd, T. P. Scott, D. V. Boger, J. J. Cooper-White, and G. H. McKinley, J. Non-Newtonian Fluid Mech. **129**(1), 1–22 (2005).
[19]J. Gachelin, G. Miño, H. Berthet, A. Lindner, A. Rousselet, and É. Clément, Phys. Rev. Lett. **110**(26), 268103 (2013).
[20]S. Rafaï, L. Jibuti, and P. Peyla, Phys. Rev. Lett. **104**(9), 098102 (2010).
[21]R. G. Larson, Rheol. Acta **31**(3), 213–263 (1992).
[22]R. W. Connelly and J. Greener, J. Rheol. **29**(2), 209–226 (1985).
[23]C. Clasen, B. P. Gearing, and G. H. McKinley, J. Rheol. **50**(6), 883–905 (2006).
[24]G. Davies and J. Stokes, J. Non-Newtonian Fluid Mech. **148**(1), 73–87 (2008).
[25]V. Sharma, A. Jaishankar, Y.-C. Wang, and G. H. McKinley, Soft Matter **7**(11), 5150–5160 (2011).
[26]A. Colin, T. M. Squires, and L. Bocquet, Soft Matter **8**(41), 10527–10529 (2012).
[27]G. M. Whitesides, Nature **442**(7101), 368–373 (2006).
[28]H. A. Stone, A. D. Stroock, and A. Ajdari, Annu. Rev. Fluid Mech. **36**, 381–411 (2004).
[29]T. M. Squires and S. R. Quake, Rev. Mod. Phys. **77**(3), 977 (2005).
[30]W. M. Gelbart and A. Ben-Shaul, J. Phys. Chem. **100**(31), 13169–13189 (1996).
[31]D. Bartolo and D. G. Aarts, Soft Matter **8**(41), 10530–10535 (2012).
[32]F. J. Galindo-Rosales, L. Campo-Deaño, F. Pinho, E. Van Bokhorst, P. Hamersma, M. Oliveira, and M. Alves, Microfluid. Nanofluid. **12**(1–4), 485–498 (2012).
[33]T. Omori, Y. Imai, K. Kikuchi, T. Ishikawa, and T. Yamaguchi, Ann. Biomed. Eng. **43**(1), 238–257 (2015).
[34]J. Dealy, Rheol. Bull. **79**(2), 14–18 (2010).
[35]T. Boronat, V. Segui, M. Peydro, and M. Reig, J. Mater. Process. Technol. **209**(5), 2735–2745 (2009).
[36]H. Kavehpour and G. McKinley, Tribol. Lett. **17**(2), 327–335 (2004).
[37]J. R. Stokes, M. W. Boehm, and S. K. Baier, Curr. Opin. Colloid Interface Sci. **18**(4), 349–359 (2013).
[38]L. E. Rodd, T. P. Scott, D. V. Boger, J. J. Cooper-White, and G. H. McKinley, Presented at the Proceedings of the XIVth International Congress on Rheology, NF24-1-NF24-4 (2004).
[39]H. Y. Gan, Y. C. Lam, N. T. Nguyen, K. C. Tam, and C. Yang, Microfluid. Nanofluid. **3**(1), 101–108 (2007).
[40]E. Lauga, M. Brenner, and H. Stone, in *Springer Handbook of Experimental Fluid Mechanics* (Springer, 2007), pp. 1219–1240.
[41]P. D. Olmsted, EPL **48**(3), 339 (1999).
[42]G. G. Fuller, *Optical Rheometry of Complex Fluids* (Oxford Univ. Press, 1995).
[43]J. Goyon, A. Colin, G. Ovarlez, A. Ajdari, and L. Bocquet, Nature **454**(7200), 84–87 (2008).
[44]G. Degré, P. Joseph, P. Tabeling, S. Lerouge, M. Cloitre, and A. Ajdari, Appl. Phys. Lett. **89**(2), 024104 (2006).
[45]K. N. Nordstrom, E. Verneuil, P. Arratia, A. Basu, Z. Zhang, A. G. Yodh, J. P. Gollub, and D. J. Durian, Phys. Rev. Lett. **105**(17), 175701 (2010).
[46]T. T. Perkins, D. E. Smith, and S. Chu, Science **276**(5321), 2016–2021 (1997).
[47]D. J. Mai, C. Brockman, and C. M. Schroeder, Soft Matter **8**(41), 10560–10572 (2012).
[48]G. F. Christopher and S. L. Anna, J. Phys. D: Appl. Phys. **40**(19), R319 (2007).
[49]S. A. Vanapalli, M. H. Duits, and F. Mugele, Biomicrofluidics **3**(1), 012006 (2009).
[50]J. B. Dahl, J.-M. G. Lin, S. J. Muller, and S. Kumar, Annu. Rev. Chem. Biomol. Eng. **6**, 293–317 (2015).
[51]S. J. Haward, M. S. Oliveira, M. A. Alves, and G. H. McKinley, Phys. Rev. Lett. **109**(12), 128301 (2012).
[52]N. Srivastava, R. D. Davenport, and M. A. Burns, Anal. Chem. **77**(2), 383–392 (2005).

[53]Y. J. Kang, S. Y. Yoon, K. H. Lee, and S. Yang, Artif. Organs **34**(11), 944–949 (2010).
[54]H. Zeng and Y. Zhao, Presented at the IEEE 22nd International Conference on Micro Electro Mechanical Systems (MEMS 2009) (2009).
[55]C. Neils, Z. Tyree, B. Finlayson, and A. Folch, Lab Chip **4**(4), 342–350 (2004).
[56]K. M. Schultz and E. M. Furst, Lab Chip **11**(22), 3802–3809 (2011).
[57]J. Lee and A. Tripathi, Anal. Chem. **77**(22), 7137–7147 (2005).
[58]D. E. Solomon and S. A. Vanapalli, Microfluid. Nanofluid. **16**(4), 677–690 (2014).
[59]L. L. Josephson, W. J. Galush, and E. M. Furst, Biomicrofluidics **10**(4), 043503 (2016).
[60]C. J. Pipe, T. S. Majmudar, and G. H. McKinley, Rheol. Acta **47**(5–6), 621–642 (2008).
[61]J. Chevalier and F. Ayela, Rev. Sci. Instrum. **79**(7), 076102 (2008).
[62]K. Kang, L. J. Lee, and K. W. Koelling, Exp. Fluids **38**(2), 222–232 (2005).
[63]R. Puers, Sens. Actuators A: Phys. **37**, 93–105 (1993).
[64]G. Blazquez, P. Pons, and A. Boukabache, Sens. Actuators **17**(3), 387–403 (1989).
[65]D. F. James and G. M. Chandler, J. Rheol. **37**(5), 893–909 (1993).
[66]S.-G. Baek and J. J. Magda, J. Rheol. **47**(5), 1249–1260 (2003).
[67]L. Pan and P. E. Arratia, Microfluid. Nanofluid. **14**(5), 885–894 (2013).
[68]S. Al-Roubaie, E. D. Jahnsen, M. Mohammed, C. Henderson-Toth, and E. A. Jones, Am. J. Physiol.-Heart Circ. Physiol. **301**(6), H2473–H2481 (2011).
[69]S. J. Haward, J. A. Odell, M. Berry, and T. Hall, Rheol. Acta **50**(11–12), 869–879 (2011).
[70]T. J. Ober, S. J. Haward, C. J. Pipe, J. Soulages, and G. H. McKinley, Rheol. Acta **52**(6), 529–546 (2013).
[71]See http://www.rheosense.com/products/viscometers/m-vroc/overview for Rheosense.
[72]S. D. Hudson, P. Sarangapani, J. A. Pathak, and K. B. Migler, J. Pharm. Sci. **104**(2), 678–685 (2015).
[73]D. E. Solomon, A. Abdel-Raziq, and S. A. Vanapalli, Rheol. Acta 1–12 (2016).
[74]G. M. Walker and D. J. Beebe, Lab Chip **2**(3), 131–134 (2002).
[75]F.-G. Tseng, C.-J. C. Kim, and C.-M. Ho, Presented at the the Eleventh Annual International Workshop on Micro Electro Mechanical Systems (MEMS 98) (1998).
[76]S. K. Cho, H. Moon, and C.-J. Kim, J. Microelectromech. Syst. **12**(1), 70–80 (2003).
[77]N. Srivastava and M. A. Burns, Anal. Chem. **78**(5), 1690–1696 (2006).
[78]N. Srivastava and M. A. Burns, Lab Chip **6**(6), 744–751 (2006).
[79]S. Vanapalli, D. Van den Ende, M. Duits, and F. Mugele, Appl. Phys. Lett. **90**(11), 114109 (2007).
[80]A. Groisman, M. Enzelberger, and S. R. Quake, Science **300**(5621), 955–958 (2003).
[81]Z. Wu and N.-T. Nguyen, Sens. Actuators B: Chem. **107**(2), 965–974 (2005).
[82]P. Guillot, P. Panizza, J.-B. Salmon, M. Joanicot, A. Colin, C.-H. Bruneau, and T. Colin, Langmuir **22**(14), 6438–6445 (2006).
[83]Y. J. Kang, E. Yeom, and S.-J. Lee, Biomicrofluidics **7**(5), 054111 (2013).
[84]Y. J. Kang and S. Yang, Microfluid. Nanofluid. **14**(3–4), 657–668 (2013).
[85]W. Lan, S. Li, J. Xu, and G. Luo, Microfluid. Nanofluid. **8**(5), 687–693 (2010).
[86]O. Bonhomme, A. Morozov, J. Leng, and A. Colin, Phys. Rev. E **83**(6), 065301 (2011).
[87]P. Guillot, T. Moulin, R. Kötitz, M. Guirardel, A. Dodge, M. Joanicot, A. Colin, C.-H. Bruneau, and T. Colin, Microfluid. Nanofluid. **5**(5), 619–630 (2008).
[88]S. Choi and J. K. Park, Small **6**(12), 1306–1310 (2010).
[89]S. A. Vanapalli, A. G. Banpurkar, D. van den Ende, M. H. Duits, and F. Mugele, Lab Chip **9**(7), 982–990 (2009).
[90]M. A. Cartas-Ayala, M. Raafat, and R. Karnik, Small **9**(3), 333–333 (2013).
[91]Z. Khan and S. Vanapalli, Biomicrofluidics **7**(1), 011806 (2013).
[92]M. Abkarian, M. Faivre, and H. A. Stone, Proc. Natl. Acad. Sci. U.S.A. **103**(3), 538–542 (2006).
[93]P. Galambos and F. Forster, *ASME Int. Mech. Eng. Cong. Exp., Anaheim*, CA (1998), pp. 187–191.
[94]P. Arosio, K. Hu, F. A. Aprile, T. Müller, and T. P. Knowles, Anal. Chem. **88**(7), 3488–3493 (2016).
[95]T. G. Mason, Rheol. Acta **39**(4), 371–378 (2000).
[96]T. A. Waigh, Rep. Prog. Phys. **68**(3), 685 (2005).
[97]T. M. Squires and T. G. Mason, Annu. Rev. Fluid Mech. **42**(1), 413 (2009).
[98]C. D. Chapman and R. M. Robertson-Anderson, Phys. Rev. Lett. **113**(9), 098303 (2014).
[99]L. Campo-Deaño, R. P. Dullens, D. G. Aarts, F. T. Pinho, and M. S. Oliveira, Biomicrofluidics **7**(3), 034102 (2013).
[100]M. Tassieri, F. Del Giudice, E. J. Robertson, N. Jain, B. Fries, R. Wilson, A. Glidle, F. Greco, P. A. Netti, and P. L. Maffettone, Sci. Rep. **5**, Article No. 8831 (2015).
[101]A. I. Bishop, T. A. Nieminen, N. R. Heckenberg, and H. Rubinsztein-Dunlop, Phys. Rev. Lett. **92**(19), 198104 (2004).
[102]S. Keen, A. Yao, J. Leach, R. Di Leonardo, C. Saunter, G. Love, J. Cooper, and M. Padgett, Lab Chip **9**(14), 2059–2062 (2009).
[103]T. Mason, H. Gang, and D. Weitz, J. Mol. Struct. **383**(1), 81–90 (1996).
[104]R. Holyst, A. Bielejewska, J. Szymański, A. Wilk, A. Patkowski, J. Gapiński, A. Żywociński, T. Kalwarczyk, E. Kalwarczyk, and M. Tabaka, Phys. Chem. Chem. Phys. **11**(40), 9025–9032 (2009).
[105]R. Lindken, M. Rossi, S. Große, and J. Westerweel, Lab Chip **9**(17), 2551–2567 (2009).
[106]A. Pipkin and R. Tanner, Annu. Rev. Fluid Mech. **9**(1), 13–32 (1977).
[107]Y.-Y. Lin, C.-W. Lin, L.-J. Yang, and A.-B. Wang, Electrochim. Acta **52**(8), 2876–2883 (2007).
[108]M. Khan, S. Schmid, P. E. Larsen, Z. J. Davis, W. Yan, E. H. Stenby, and A. Boisen, Sens. Actuators B: Chem. **185**, 456–461 (2013).
[109]G. Dehestru, M. Leman, J. Jundt, P. Dryden, M. Sullivan, and C. Harrison, Rev. Sci. Instrum. **82**(3), 035113 (2011).
[110]M. Assael, C. Oliveira, M. Papadaki, and W. Wakeham, Int. J. Thermophys. **13**(4), 593–615 (1992).
[111]M. Youssry, E. Lemaire, B. Caillard, A. Colin, and I. Dufour, Meas. Sci. Technol. **23**(12), 125306 (2012).
[112]E. Livak-Dahl, J. Lee, and M. A. Burns, Lab Chip **13**(2), 297–301 (2013).
[113]M. F. DeLaMarre, A. Keyzer, and S. A. Shippy, Anal. Chem. **87**(9), 4649–4657 (2015).
[114]S.-Y. Teh, R. Lin, L.-H. Hung, and A. P. Lee, Lab Chip **8**(2), 198–220 (2008).

[115]R. Mukhopadhyay, Anal. Chem. **77**(21), 429A–432A (2005).
[116]F. Del Giudice, F. Greco, P. A. Netti, and P. L. Maffettone, Biomicrofluidics **10**(4), 043501 (2016).
[117]T. Gervais, J. El-Ali, A. Günther, and K. F. Jensen, Lab Chip **6**(4), 500–507 (2006).
[118]A. A. Yazdi, A. Popma, W. Wong, T. Nguyen, Y. Pan, and J. Xu, Microfluid. Nanofluid. **20**(3), 1–18 (2016).
[119]W. S. Wang and S. A. Vanapalli, Biomicrofluidics **8**(6), 064111 (2014).
[120]G. Lowe, A. Rumley, J. Norrie, I. Ford, J. Shepherd, S. Cobbe, P. Macfarlane, and C. Packard, Thromb. Haemostasis **84**(4), 553–558 (2000).
[121]S. K. Lai, Y.-Y. Wang, D. Wirtz, and J. Hanes, Adv. Drug Delivery Rev. **61**(2), 86–100 (2009).
[122]I. Reimann, Clin. Orthop. Relat. Res. **119**, 237–241 (1976).
[123]M. Sun, S. S. Bithi, and S. A. Vanapalli, Lab Chip **11**(23), 3949–3952 (2011).
[124]B. Bhattacharjee and S. A. Vanapalli, Biomicrofluidics **8**(4), 044111 (2014).
[125]S. S. Bithi, W. S. Wang, M. Sun, J. Blawzdziewicz, and S. A. Vanapalli, Biomicrofluidics **8**(3), 034118 (2014).
[126]M. Sun and S. A. Vanapalli, Anal. Chem. **85**(4), 2044–2048 (2013).
[127]J. Zilz, C. Schäfer, C. Wagner, R. J. Poole, M. A. Alves, and A. Lindner, Lab Chip **14**(2), 351–358 (2014).
[128]F. Del Giudice, G. D'Avino, F. Greco, I. De Santo, P. A. Netti, and P. L. Maffettone, Lab Chip **15**(3), 783–792 (2015).
[129]P. Bhattacharjee, A. McDonnell, R. Prabhakar, L. Yeo, and J. Friend, New J. Phys. **13**(2), 023005 (2011).
[130]B. Keshavarz, V. Sharma, E. C. Houze, M. R. Koerner, J. R. Moore, P. M. Cotts, P. Threlfall-Holmes, and G. H. McKinley, J. Non-Newtonian Fluid Mech. **222**, 171–189 (2015).
[131]R. Besseling, L. Isa, E. R. Weeks, and W. C. Poon, Adv. Colloid Interface Sci. **146**(1), 1–17 (2009).
[132]J. Katz and J. Sheng, Annu. Rev. Fluid Mech. **42**, 531–555 (2010).
[133]J. Huisken, J. Swoger, F. Del Bene, J. Wittbrodt, and E. H. Stelzer, Science **305**(5686), 1007–1009 (2004).
[134]L. Hall-Stoodley, J. W. Costerton, and P. Stoodley, Nat. Rev. Microbiol. **2**(2), 95–108 (2004).
[135]M. N. Hatton, M. J. Levine, J. E. Margarone, and A. Aguirre, J. Oral Maxillofac. Surg. **45**(6), 496–499 (1987).
[136]B. A. Inman, W. Etienne, R. Rubin, R. A. Owusu, T. R. Oliveira, D. B. Rodriques, P. F. Maccarini, P. R. Stauffer, A. Mashal, and M. W. Dewhirst, Int. J. Hyperthermia **29**(3), 206–210 (2013).
[137]M. Anand and K. Rajagopal, Int. J. Cardiovasc. Med. Sci **4**(2), 59–68 (2004).
[138]G. Késmárky, P. Kenyeres, M. Rábai, and K. Tóth, Clin. Hemorheol. Microcirc. **39**(1–4), 243–246 (2008).
[139]A. N. Ketene, E. M. Schmelz, P. C. Roberts, and M. Agah, Nanomed.: Nanotechnol. Biol. Med. **8**(1), 93–102 (2012).
[140]S. Moreno-Flores, R. Benitez, M. Vivanco, and J. L. Toca-Herrera, Nanotechnology **21**(44), 445101 (2010).